Article

Maternal behavior promotes resilience to adolescent stress in mice through a microglia-neuron axis

Hongyu Chen[1,2,8], Ruifeng Xu[1,2,3,8], Jianhao Wang[1,2,8], Feng Gao[1,2,8], Yida Lv[1,2], Xiang Li[1,2], Fang Li[1,2], Junqin Zhao[1,2], Xi Zhang[1,2], Jiabei Wang[1,2], Ruicheng Du[1,2], Yuke Shi[1,2], Hang Yu[1,2], Shuai Ding[1,2], Wenxin Li[1,2], Jing Xiong [1,2], Jie Zheng[4,5], Liang Zhao[3], Xin-Ya Gao[6,7] & Zhi-Hao Wang [1,2] ✉

Early life experience modulates resilience to stress in later life. Previous research implicated maternal care as a key mediator of behavioral responses to the adversity in adolescence, but details of molecular mechanisms remain elusive. Here, we show social stress activates transcription factor C/EBPβ in mPFC neurons of adolescent mice, which transcriptionally upregulates *Dnm1l* and promotes mitochondrial dysfunction, thereby conferring stress suscept-ibility in adolescent mice. Moreover, different maternal separation differen-tially regulates adolescent stress susceptibility. Mechanistically, this differential effect depends on maternal behavior-stimulated IGF-1, which inhibits neuronal C/EBPβ through mTORC1-induced C/EBPβ-LIP translation. Furthermore, we identify maternal behavior-stimulated IGF-1 is mainly released from mPFC microglia. Notably, increased maternal care under an environmental enrichment condition or maternal behavior impairment induced by repeated MPOA[Esr1+] cells inhibition in dams prevents or promotes stress susceptibility via microglial-to-neuronal IGF-1-C/EBPβ-DRP1 signaling. In this work, these findings have unveiled molecular mechanisms by which maternal behavior promotes stress resilience in adolescents.

Adolescence is a unique period of growth and turmoil[1]. Adolescent stress and trauma (including bullying and a range of family events) are associated with the onset of psychiatric disorders such as major depressive disorder (MDD)[2,3]. The onset of depression peaks in adolescence[4–6], with 34% of the world's population aged 10–19 years at risk of clinical depression[7]. Depression is a leading cause of disability in adolescents, but the effectiveness of treatments for adolescent depression is limited due to a lack of understanding of the neurobio-logical mechanisms of the disease[8].

Notably, some adolescents maintain normal physiological and behavioral functioning in the face of extraordinary stress, a process known as resilience[9]. Currently, there are fewer studies on adolescent animal models of resilience compared to those conducted on adult models[10,11], but there is an urgent need to determine the detailed

[1]Department of Neurology, Renmin Hospital of Wuhan University, Wuhan, China. [2]Center for Neurodegenerative Disease Research, Renmin Hospital of Wuhan University, Wuhan, China. [3]Department of Thoracic Surgery, National Cancer Center/National Clinical Research Center for Cancer/Cancer Hospital, Chinese Academy of Medical Sciences and Peking Union Medical College, Beijing, China. [4]Neuroscience Research Institute and Department of Neurobiology, School of Basic Medical Sciences, Peking University, Beijing, China. [5]Key Laboratory for Neuroscience, Ministry of Education/National Health Commission, Peking University, Beijing, China. [6]Department of Neurology, Henan Provincial People's Hospital, Zhengzhou, China. [7]Laboratory of Neurology, Henan Provincial People's Hospital, Zhengzhou, China. [8]These authors contributed equally: Hongyu Chen, Ruifeng Xu, Jianhao Wang, Feng Gao. ✉e-mail: wangzh86@whu.edu.cn

mechanisms of adolescent resilience in order to understand the pathogenesis of adolescent psychiatric disorders and to identify therapeutic targets and approaches.

Epidemiological and preclinical studies have shown that adolescents' resilience to stressful events in later life can be impaired by severe early life stressors, such as an adverse postnatal environment[12–15]. Thus, a "two-hit" stress model has been linked to the development of depression by suggesting that environmental insults during the postpartum period (the first hit) prime an individual's psychopathology after subsequent insults later in life (the second hit)[16–19]. However, the molecular mechanisms by which early life experiences, particularly during the postpartum period, influence stress resilience in adolescents remain unclear. The postpartum period is the most critical stage in an individual's life and the time when the offspring is most in need of maternal care[20]. In rodents, maternal behavior alters the offspring epigenome in the hippocampus[21], affects the offspring hippocampal transcriptome[22], and drives somatic variation in the offspring genome[23]. Importantly, mice that experience disrupted maternal care in a model of maternal separation (MS) are more susceptible to late-life chronic stress and developed depression-like behaviors[16,24,25], indicating that maternal care is important for behavioral responses to the late-life adversity. These findings suggest that maternal care affects the offspring behavioral and socioemotional outcomes. However, due to the lack of effective approaches to precisely modulate maternal behavior, it is inconclusive whether and how changes in the level of maternal behavior during the postnatal period affect the vulnerability of offspring to stress in adolescence.

Regarding mechanistic studies, mitochondrial dysfunction has been identified as a risk factor for both adult and adolescent MDD[26–28]. There is evidence for reduced mitochondrial oxidative phosphorylation in the glutamatergic neurons of patients with depression[29]. In addition, increased mitochondrial fission has been observed in adult mice susceptible to chronic social defeat stress (CSDS), resulting in a large number of tiny mitochondria with low ATP production[30]. Although the role of mitochondrial dysfunction in adult stress susceptibility is becoming clearer[30–33], to our knowledge there is little preclinical research that mechanistically explains the link between adolescent stress susceptibility and mitochondrial dysfunction.

In this work, we show that neuronal Dynamin-Related Protein 1 (DRP1, gene name *Dnm1l*), which mediates mitochondrial fission, is transcriptionally upregulated by the transcription factor CCAAT/ enhancer binding protein β (C/EBPβ) in the medial prefrontal cortex (mPFC) in a mouse model of adolescent stress vulnerability. Furthermore, using a combination of chemogenetic modulation of maternal behavior and specific targeting of microglia and neurons, we demonstrate that maternal behavior promotes the release of insulin-like growth factor-1 (IGF-1) from microglia in pups, which in turn inhibits the transcriptional activity of C/EBPβ through the IGF-1 receptor (IGF-1R)/mTORC1 pathway-stimulated C/EBPβ-LIP (liver inhibitory protein) translation in the neuron and promotes resilience to stress in adolescent mice, indicating a significant protective effect of maternal behavior during postpartum period against adolescent depression.

Results

Social defeat stress induces mitochondrial dysfunction in the mPFC of the adolescent susceptible mice
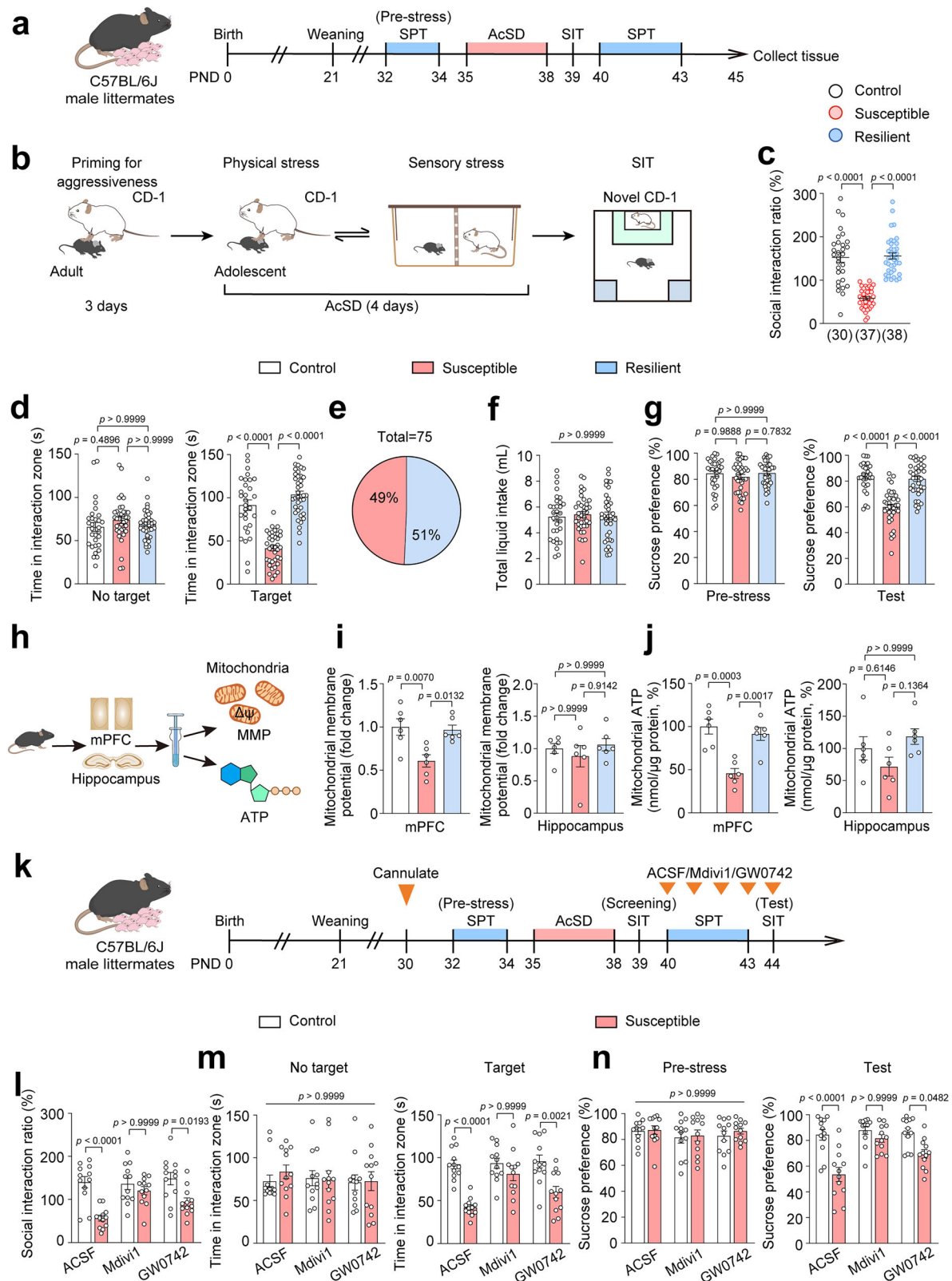
To investigate the pathogenesis of adolescent depression, we used the accelerated social defeat stress (AcSD) paradigm in C57BL/6J wild-type (WT) mice, a well-established model to allow exposure during discrete periods of adolescence for both male and female (Fig. 1a, b, Supplementary Fig. 1a)[10,11,34]. Given that the prevalence of adolescent depression typically peaks in mid-adolescence[35,36], we performed AcSD and the social interaction test (SIT) on WT mice aged 35–44 days. Through the AcSD and SIT experiments, we identified susceptible ($n = 37$) and resilient ($n = 38$) mice, with 49% susceptible and 51%

resilient in male mice (Fig. 1c–e). Importantly, susceptible mice had a lower sucrose preference compared to control and resilient mice, with no significant differences in basal measurements or total fluid intake (Fig. 1f–g). Similar results were observed in female mice (Supplementary Fig. 1b–d).

Since mitochondrial dysfunction is one of the key mechanisms in adult depression[37], we measured mitochondrial function in WT mice after exposure to AcSD or control to determine the relevance of mitochondrial damage to adolescent stress susceptibility (Fig. 1h). The results showed that mitochondrial membrane potential (MMP) and ATP levels in the mPFC were significantly decreased in susceptible male and female mice, whereas they were not significantly decreased in the hippocampus (Fig. 1i, j, Supplementary Fig. 1e, f). The above results suggest that stress induces mitochondrial dysfunction in the mPFC of adolescent depression-like mice with no sex difference.

Subsequently, we asked which aspect of mitochondrial dysfunction was responsible for adolescent depression. To answer this question, we injected two mitochondrial modulators, the mitochondrial fission inhibitor Mdivi1 and the peroxisome proliferator-activated receptor-δ (PPAR-δ) agonist GW0742, into susceptible mice (Fig. 1k)[30,31]. The placement of cannula was shown in Supplementary Fig. 2a. Interestingly, Mdivi1 effectively alleviated both social avoidance and anhedonia behaviors induced by AcSD, whereas GW0742 did not produce similar effects (Fig. 1l–n). Additionally, we performed open-field test and elevated plus maze test in control and susceptible mice after injection, and showed that manipulation of Mdivi1 or GW0742 did not affect locomotion and anxiety-related behaviors in adolescent mice (Supplementary Fig. 2b, c). We further tested the MMP and mitochondrial ATP levels in mPFC of control and susceptible mice injected with ACSF, Mdivi1, or GW0742. The results showed that AcSD-induced mitochondrial dysfunction was rescued by Mdivi1, but not GW0742, indicating Mdivi1 restored AcSD-induced social interaction and sucrose preference through affecting MMP and mitochondrial ATP levels (Supplementary Fig. 2d, e). In addition, electron microscope images showed a bimodal distribution of mitochondrial fission sites. In the mPFC of susceptible mice injected with ACSF, the relative distance from fission sites to the tip of mitochondria was about 25%, whereas the relative distance was ~50% in the mPFC of control mice injected with ACSF (Supplementary Fig. 2f, h). Only Mdivi1 significantly improved mitochondrial morphology, that is, the relative distance from the mitochondrial fission point to the tip was similar in Mdivi1-injected control and Mdivi1-injected susceptible mice (Supplementary Fig. 2f, h). Besides, the number of tiny mitochondria in the mPFC of susceptible mice injected with ACSF or GW0742 was increased, whereas the number of tiny mitochondria in the mPFC of susceptible mice injected with Mdivi1 did not change significantly (Supplementary Fig. 2g, i). These results suggest that Mdivi1 but not GW0742 affects mitochondrial fission. Considering that Mdivi1 is a proven inhibitor of mitochondrial fission that prevents mitochondrial division by blocking DRP1 self-assembly[38], we further assessed whether Mdivi1 or GW0742 had an effect on DRP1 expression in mPFC. The results showed that Mdivi1 (but not GW0742) significantly suppressed the elevated levels of p-DRP1 and DRP1 in susceptible mice (Supplementary Fig. 2j, k). This result suggests that Mdivi1 attenuates the expression of DRP1 in mPFC of adolescent susceptible mice, whereas GW0742 does not.

To clarify the role of DRP1 in the adolescent stress susceptibility, we further examined the protein expression and mRNA levels of DRP1 in AcSD mice. The results from male mice showed that both phosphorylated and total DRP1 protein expressions were upregulated in the mPFC of susceptible group after AcSD, whereas no significant upregulation was seen in the hippocampus (Fig. 2a, b, Supplementary Fig. 3a, b). Moreover, *Dnm1l* mRNA levels were also elevated only in the mPFC of susceptible mice (Fig. 2c *left*, Supplementary Fig. 3c). Interestingly, increased *Dnm1l* mRNA levels in the mPFC were negatively

correlated with the social interaction ratio (Fig. 2c *right*). Similar changes in DRP1 levels were observed in female mice, indicating that the observed effect is not sex-specific (Supplementary Fig. 3d–f).

Furthermore, to confirm the link between DRP1 and depression-like behaviors in adolescent mice, we performed 1-, 2-, 3- and 4-day AcSD, which resulted in an increase in protein expression and mRNA levels of DRP1 in a time-dependent manner (Supplementary Fig. 3g–j).

Notably, only a 4-day AcSD (standard course) resulted in a reduction in the social interaction ratio in adolescent mice (Supplementary Fig. 3k). Additionally, the classic antidepressant fluoxetine (FLX) effectively reversed the AcSD-induced increase in DRP1 protein expression and mRNA levels, and restored the social interaction ratio (Supplementary Fig. 3l–p). In another depression paradigm, chronic unpredictable stress (CUS), there was also an increase in DRP1 protein expression and

Fig. 1 | Social defeat stress induces mitochondrial dysfunction in the mPFC of the adolescent susceptible mice. a Schematic representation of the AcSD experimental course and behavioral test process for C57BL/6J male mice. SPT, sucrose preference test; AcSD, accelerated social stress defeat; SIT, social interaction test. **b** Graphic representation of AcSD stress paradigm for adolescent mice. **c** Scatter plot depicting the distribution of social interaction ratio for control (without experiencing AcSD), susceptible (ratio < 100), and resilient (ratio ≥ 100) after the AcSD paradigm. The white, red, and blue dots represent the control, susceptible, and resilient groups, respectively. **d** Measurement of the time in interaction zone of the above mice without or with target. **e** The percentages of susceptible (red) and resilient (blue) mice exposed to AcSD. Measurement of the total liquid intake (**f**) and the percentage of sucrose consumption (**g**) in SPT. Data in (**c**–**g**) are presented as the mean ± SEM (n = 30 mice for the control group, n = 37 mice for the susceptible group, n = 38 mice for the resilient group; one-way ANOVA and Bonferroni's multiple comparison test). **h** Graphic representation of

mitochondrial membrane potential (MMP) and ATP levels in the mPFC and the hippocampus of adolescent mice. Measurement of mitochondrial MMP (**i**) and ATP levels (**j**) in the mPFC and the hippocampus from WT male mice exposed to AcSD or control. Data in (**i**, **j**) are presented as the mean ± SEM (n = 6 for each group; one-way ANOVA and Bonferroni's multiple comparison test). **k** Schematic representation of the experimental procedure for AcSD paradigm and behavioral test process for C57BL/6J male mice with administration of Mdivi1, GW0742 or ACSF (Artificial Cerebrospinal Fluid). **l**–**n** Behavioral tests of WT male mice exposed to AcSD paradigm with administration of Mdivi1, GW0742 or ACSF. Measurement of social interaction ratio (**l**), time in interaction zone without or with target (**m**), and the percentage of sucrose preference (**n**) in WT male mice with indicative treatments. Data in (**l**–**n**) are presented as the mean ± SEM (n = 12 mice for each group; one-way ANOVA and Bonferroni's multiple comparison test). See also Supplementary Figs. 1, 2. Source data are provided as a Source Data file.

mRNA levels (Supplementary Fig. 3q–s). These results demonstrate that DRP1 is closely associated with adolescent depression-like behaviors in mice. Taken together, we conclude that DRP1 plays a crucial role in mediating mitochondrial function in the mPFC and promoting depression-like behaviors in adolescent mice following social defeat stress. To further determine the relationship between *Dnm1l* level and MDD in human samples, we screened dorsolateral prefrontal cortex samples from patients with MDD in the GEO database and selected the dataset GSE54568, which consists of 15 samples from MDD patients and 15 samples from non-psychiatric controls. The results showed a higher relative expression of *Dnm1l* in the dorsolateral prefrontal cortex of depressed patients compared to controls (p = 0.0633) (Supplementary Fig. 4a).

Neuronal DRP1 in the mPFC contributes to stress susceptibility in adolescent mice
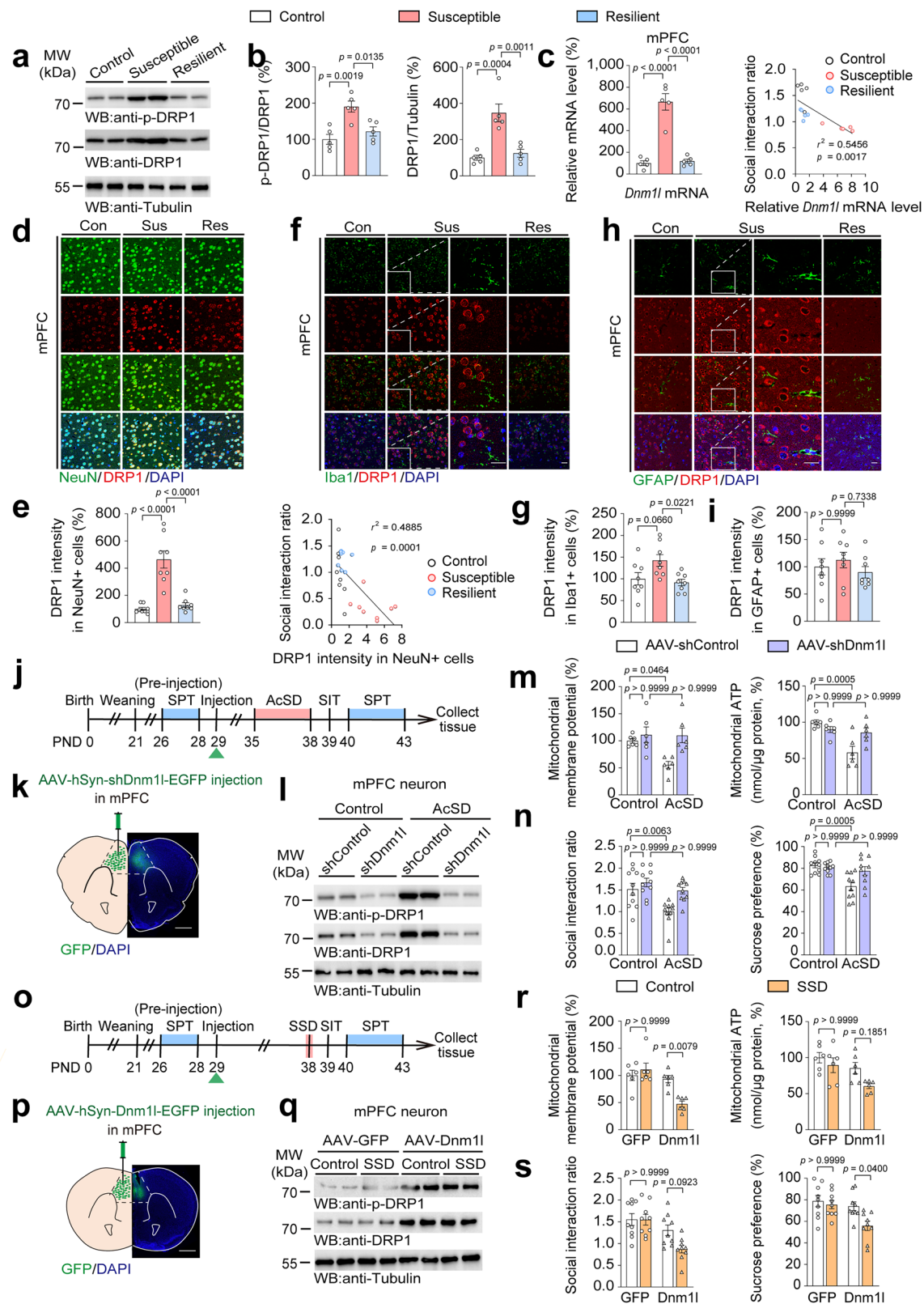
We further asked that DRP1 contribute to adolescent depression in which cell type of mPFC. We performed co-immunostaining of DRP1 with neuronal (NeuN), microglial (Iba1) and astrocytic (GFAP) markers on brain slices of WT mice undergoing AcSD paradigm, respectively. DRP1 was observed to be highly co-localized with NeuN in the mPFC of adolescent susceptible mice (Fig. 2d–i). Importantly, DRP1 intensity in NeuN+ cells was negatively correlated with the social interaction ratio, highlighting the involvement of neuronal DRP1 in the mPFC for depressive-like behavior in adolescent mice (Fig. 2e, *right*). Next, to further understand the causal effect of DRP1 on depressive-like behavior in adolescents, we injected AAV-hSyn-shDnm1l-EGFP or AAV-hSyn-shControl-EGFP into the mPFC of WT mice at PND 29 to knockdown neuronal DRP1 (Fig. 2j). Immunostaining and Western blotting confirmed the validity of viral knockdown (Fig. 2k, l, Supplementary Fig. 5a–c). Notably, specific reduction of DRP1 not only restored mitochondrial function disrupted by AcSD, but also significantly improved social interaction ratio and sucrose preference without affecting basal measurements (Fig. 2m, n, Supplementary Fig. 5d, e). In addition, to assess the effect of DRP1 upregulation, we applied AAV-hSyn-Dnm1l-EGFP or AAV-hSyn-EGFP to specifically overexpress neuronal DRP1 in the mPFC with a subthreshold social defeat stress (SSD) paradigm (Fig. 2o). Immunostaining and Western blotting also confirmed the viral efficiency (Fig. 2p, q, Supplementary Fig. 5f–h). Neuronal overexpression of DRP1 induced mitochondrial dysfunction in the mPFC of SSD mice, suggesting that upregulated DRP1 confers mitochondrial disturbances (Fig. 2r). Unsurprisingly, SSD was not sufficient to induce behavioral deficits in social interaction and sucrose preference in control mice. However, mice overexpressing DRP1 in the mPFC neurons showed significantly reduced social interactions and sucrose preference after SSD, indicating that increased DRP1 in the mPFC neurons exacerbates stress susceptibility in adolescent mice (Fig. 2s, Supplementary Fig. 5i, j). These results illustrate that DRP1-

related mitochondrial dysfunction in the mPFC neurons is required for stress susceptibility in adolescent mice.

Neuronal C/EBPβ acts as a transcription activator for *Dnm1l* and regulates stress susceptibility in adolescent mice

Why is neuronal DRP1 expression upregulated in mPFC neurons under adolescent stress? We hypothesized that there may be transcriptional regulation of DRP1 based on previously observed changes in *Dnm1l* mRNA levels. Using the ChIP-Atlas data provided by the Signaling Pathways Project (SPP), we screened several transcription factors based on their binding scores in HeLa S3 cells, including *Gabpa*, *Ctcf*, *Rest*, and *Cebpb* (Fig. 3a). Subsequently, we assessed the mRNA levels of these four transcription factors in control and susceptible mice, and the results showed that only *Cebpb* mRNA levels were significantly elevated in susceptible mice compared to control mice (Fig. 3b). Notably, this increase in *Cebpb* mRNA levels was unique to the susceptible mice, and no similar changes were observed in the control or resilient groups (Supplementary Fig. 6a). Furthermore, an inverse correlation was found between *Cebpb* mRNA levels and social interaction ratios (Fig. 3c). Consistently, protein analysis of mPFC revealed parallel increases in both phosphorylated and total C/EBPβ exclusively in the susceptible mice (Fig. 3d, Supplementary Fig. 6b). Further analyses utilizing fluorescence in situ hybridization (FISH) with immunostaining revealed that both p-C/EBPβ and *Dnm1l* mRNA levels were elevated at cellular level in the mPFC of susceptible mice and that there was a significant negative correlation between the intensity of p-C/EBPβ and the rate of social interaction (Fig. 3e, f, Supplementary Fig. 6c, d). Our results indicated p-C/EBPβ is highly correlated with *Dnm1l* mRNA as a high intensity of p-C/EBPβ with more *Dnm1l* mRNA was detected in solid-lined circles, and there was a low intensity of p-C/EBPβ with little *Dnm1l* mRNA in dotted-lined circles (Fig. 3e, g). Immunostaining further confirmed that C/EBPβ intensity was significantly increased in susceptible mice and positively correlated with DRP1 intensity (Fig. 3h–j). Moreover, we have further analyzed *Cebpb* mRNA levels in the dataset used in the manuscript and showed that *Cebpb* mRNA levels tended to be elevated in postmortem depressed brains, which was similar to the *Dnm1l* mRNA trend (Supplementary Fig. 6e). These findings indicate C/EBPβ may act as a transcriptional regulator of DRP1 in the mPFC of susceptible mice.

Subsequently, to substantiate the transcriptional role of C/EBPβ, we analyzed ChIP-seq data from Cistrome, which revealed that C/EBPβ had high binding scores in the *Dnm1l* promoter region in different cell lines (Fig. 3k). After DNA sequence analysis reported several possible C/EBPβ-binding motifs, we conducted full-length and different truncations of the *Dnm1l* promoters and co-transfected them with GST or

GST-C/EBPβ for luciferase assay (Fig. 3l). The results showed that the truncated −1060 to +99 fragment displayed the lowest promoter activity, whereas the −2000 to −1061 and −1369 to +99 fragments showed enhanced activities, suggesting the site within the −1369 to −1060 fragment (Site 4) might serve as the major positive C/EBPβ binding site (Fig. 3l). Western bolting showed a consistent expression of GST-C/EBPβ (Fig. 3m, Supplementary Fig. 6f). Then, promoter

activity was significantly repressed when the truncated −2000 to −1061 fragment and full-length promoter were co-transfected with small interference si-C/EBPβ (Fig. 3n). Based on the motifs of C/EBPβ, we confirmed the homology of the human and mouse *Dnm1l* promoter sequences (Fig. 3o). Next, to further explore whether C/EBPβ directly interacts with the DNA sequence of the *Dnm1l* promoter, we designed hot, cold, and mutant probes based on Site 4, and performed
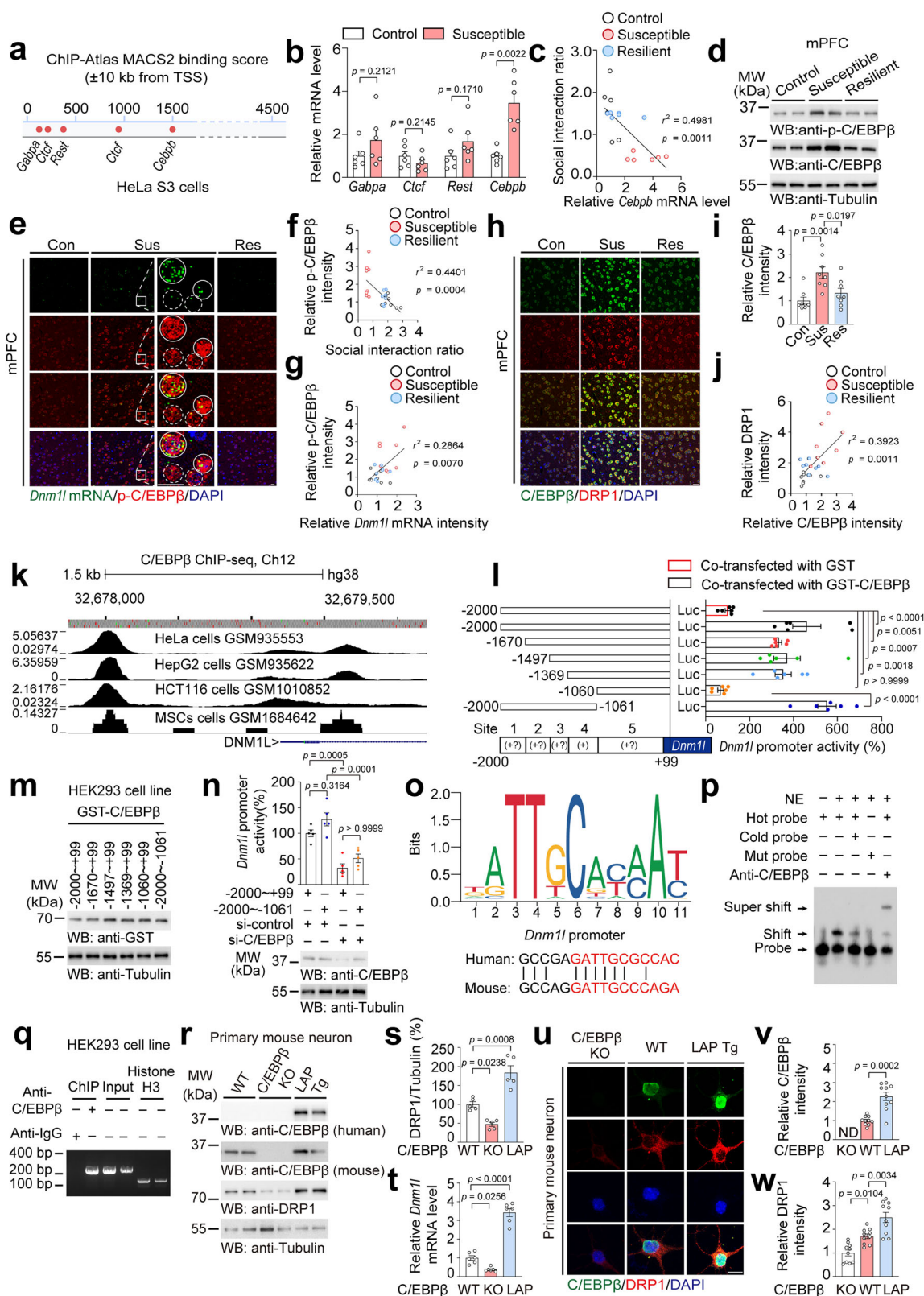
Fig. 2 | Neuronal DRP1 in the mPFC contributes to stress susceptibility in adolescent mice. a Western blotting showing the levels of p-DRP1 and DRP1 expression in the mPFC of adolescent mice after AcSD. Data are representative of three independent experiments. **b** Quantification of p-DRP1/DRP1, DRP1/Tubulin protein levels in the mPFC of adolescent mice after AcSD. **c** Measurement of *Dnm1l* mRNA levels in the mPFC of the above mice; Correlation analysis between social interaction ratio and relative *Dnm1l* mRNA levels in the mPFC of the above mice. The white, red, and blue dots represent the control, susceptible, and resilient groups, respectively. The Spearman correlation coefficient r^2 and *p* value are shown. Data in (**b**, **c**) are presented the mean ± SEM ($n = 5$ for each group; one-way ANOVA and Bonferroni's multiple comparison test). **d** Immunofluorescence co-staining of NeuN (green) and DRP1 (Red) on the brain sections of the mPFC from indicative mice exposed to AcSD. Scale bars: 20 μm. **e** Quantification of DRP1 intensity in NeuN+ cells in the mPFC from indicative mice exposed to AcSD; Correlation analysis between social interaction ratio and DRP1 intensity in NeuN+ cells in the above mice. The white, red, and blue dots represent the control, susceptible, and resilient groups, respectively. The Spearman correlation coefficient r^2 and *p* value are shown. Data are presented the mean ± SEM ($n = 8$ for each group; one-way ANOVA and Bonferroni's multiple comparison test). **f** Immunofluorescence co-staining of Iba1 (green) and DRP1 (Red) on the brain sections of the mPFC from indicative mice exposed to AcSD. Scale bars: 20 μm. **g** Quantification of DRP1 intensity in Iba1+ cells in the mPFC from indicative mice exposed to AcSD. **h** Immunofluorescence co-staining of GFAP (green) and DRP1 (Red) on the brain sections of the mPFC from indicative mice exposed to AcSD. Scale bars: 20 μm. **i** Quantification of DRP1 intensity in GFAP+ cells in the mPFC from indicative mice exposed to AcSD. Data in (**g**, **i**) are presented the mean ± SEM ($n = 8$ for each group; one-way ANOVA and Bonferroni's multiple comparison test). **j** Schematic representation of the experimental procedure for AcSD paradigm and behavioral test process for WT mice, with virus injection of AAV-hSyn-shControl-EGFP or AAV-hSyn-shDnm1l-EGFP. **k** The location of the cannula tips and fluorescence microscopy image of representative field showed GFP expression in the mPFC injected with AAV-hSyn-shDnm1l-EGFP. Scale bar: 500 μm. $n = 3$ mice for each group. **l** Representative immunoblots of p-DRP1 and DRP1 protein levels in the mPFC neurons of WT mice exposed to Control or AcSD paradigm with virus injection of AAV-hSyn-shControl-EGFP or AAV-hSyn-shDnm1l-EGFP. Data are representative of three independent experiments. **m** Measurement of mitochondrial MMP and ATP levels in the mPFC of WT mice with indicative treatments. Data are presented the mean ± SEM ($n = 6$ for each group; one-way ANOVA and Bonferroni's multiple comparison test). **n** Measurement of social interaction ratio and the percentage of sucrose preference in WT mice with indicative treatments. Data are presented the mean ± SEM ($n = 10$ mice for each group; one-way ANOVA and Bonferroni's multiple comparison test). **o** Schematic representation of the experimental procedure for SSD paradigm and behavioral test process for WT mice, with virus injection of AAV-hSyn-EGFP or AAV-hSyn-Dnm1l-EGFP. **p** The location of the cannula tips and fluorescence microscopy image of representative field showed GFP expression in the mPFC injected with AAV-hSyn-Dnm1l-EGFP. Scale bar: 500 μm. $n = 3$ mice for each group. **q** Representative immunoblots of p-DRP1 and DRP1 protein levels in the mPFC neurons of WT mice exposed to Control or SSD paradigm with virus injection of AAV-hSyn-EGFP or AAV-hSyn-Dnm1l- EGFP. Data are representative of three independent experiments. **r** Measurement of mitochondrial MMP and ATP levels in the mPFC of WT mice with indicative treatments. Data are presented the mean ± SEM ($n = 6$ for each group; one-way ANOVA and Bonferroni's multiple comparison test). **s** Measurement of social interaction ratio and the percentage of sucrose preference in WT mice with indicative treatments. Data are presented the mean ± SEM ($n = 9$ mice for each group; one-way ANOVA and Bonferroni's multiple comparison test). See also Supplementary Figs. 3–5. Source data are provided as a Source Data file.

electrophoretic mobility shift assay (EMSA). The EMSA result showed that hot probe specifically bound to the nuclear extract containing C/EBPβ, which was stripped by the cold probe or the mut probe, and this binding could be recognized by anti-C/EBPβ antibody and showed super shift (Fig. 3p). In addition, we performed a chromatin immuno-precipitation (ChIP) assay to ensure that C/EBPβ specifically binds to the *Dnm1l* promoter in vivo, significantly more than the IgG control (Fig. 3q). Moreover, C/EBPβ has three different protein isoforms by substituting translation initiation sites), LAP* (liver activating protein), LAP and LIP (liver inhibitory protein)[39]. The isoforms LAP* and LAP are transcriptional activators consisting of a transcriptional activation domain and a DNA binding domain. The truncated isomer LIP lacks the N-terminal transcription activation domain but still has a DNA-binding domain and can act as a competitive inhibitor of LAP* or LAP function[39]. Therefore, we utilized the C/EBPβ LAP Tg mice by over-expressing LAP isoform with a Thy1 promoter[40], to mimic the over-activated C/EBPβ in the neurons. Western blotting showed that LAP mice mainly expressed human LAP isoform and to a lesser extent LIP (Supplementary Fig. 6g). HEK293 cell lysates were used as positive controls. Furthermore, in mouse primary cortical neurons, mouse C/EBPβ knockout reduced the mRNA and protein levels of DRP1, which were increased in C/EBPβ LAP Tg mice, as demonstrated by Western blotting and immunostaining (Fig. 3r–w). Importantly, mRNA levels of *Dnm1l* and *Cebpb* increased in a time-dependent manner during brain development in adolescent mPFC (Supplementary Fig. 6h). In conclusion, these data support that C/EBPβ selectively binds and activates the *Dnm1l* promoter, confirming its role as a transcriptional activator for *Dnm1l*.

Since C/EBPβ exerts a positive transcriptional effect on DRP1, we next investigated in which cell type this effect is exerted. Co-immunostaining showed that the intensity of C/EBPβ was strongly co-localized with NeuN, especially in the mPFC of susceptible mice, where NeuN+ cells exhibited the highest C/EBPβ intensity (Fig. 4a, b). Furthermore, C/EBPβ intensity in NeuN+ cells was negatively correlated with the social interaction ratio (Fig. 4c). These results suggest that C/EBPβ acts as a transcription factor for DRP1 mainly in mPFC neurons. To further elucidate the effects of neuronal C/EBPβ on depressive-like behaviors in adolescence, we bred WT (C/EBPβ+/+), C/EBPβ heterozygous knockout (C/EBPβ+/-) mice and Thy1-human C/EBPβ LAP transgenic (LAP Tg) mice which express human C/EBPβ LAP, the main active isoform, specifically in neurons. First, AAV-hSyn-EGFP or AAV-hSyn-Dnm1l-EGFP was injected into the mPFC of C/EBPβ +/- and WT mice, followed by AcSD paradigm, behavioral assessment, and mitochondrial function assays (Fig. 4d). Viral and genetic manipulations were verified by immunostaining and Western blotting (Fig. 4e–g, Supplementary Fig. 7a, b). Consistent with these results, neuronal DRP1 protein levels were significantly reduced in C/EBPβ+/- mice mPFC (Fig. 4f, g *right*). Compared to WT mice, C/EBPβ +/- mice showed improved mitochondrial membrane potential and mitochondrial ATP levels after exposure to AcSD, but these improvements were reversed by overexpression of neuronal DRP1, highlighting the fact that knockdown of C/EBPβ in the mPFC alleviates AcSD-induced mitochondrial dysfunction by down-regulating DRP1 expression (Fig. 4h, i). Moreover, C/EBPβ+/- mice exhibited increased social interaction ratio and sucrose preference, which was absent when neuronal DRP1 was overexpressed, indicating that reducing C/EBPβ in the mPFC diminishes stress susceptibility in adolescent mice (Fig. 4j, k). Next, AAV-hSyn-shDnm1l-EGFP or AAV-hSyn-shControl-EGFP was administered into the mPFC of LAP Tg and WT mice, followed by SSD or control treatment (Fig. 4m). Virus and genetic efficiencies were confirmed via immunostaining and Western blotting (Fig. 4l, n, o, Supplementary Fig. 7c, d). As expected, SSD upregulated DRP1 protein expression in LAP Tg mice but not in WT mice (Fig. 4n, o *right*). Furthermore, SSD-induced mitochondrial dysfunction in the LAP Tg mice was alleviated by DRP1 knockdown in the mPFC neurons, implicating that neuronal C/EBPβ exacerbates mitochondrial dysfunction by upregulating DRP1 (Fig. 4p, q). Similarly, deficits in social behavior and sucrose preference were only observed in the SSD-treated LAP Tg mice, suggesting overexpression of neuronal C/EBPβ increases the susceptibility of depressive-like behaviors in adolescent mice (Fig. 4r, s). We further performed in vivo ChIP assays in the mPFC of WT, LAP Tg and C/EBPβ +/-

adolescent mice using the same primers as in Fig. 3q. The results showed that compared with WT mice, C/EBPβ binding to the *Dnm1l* promoter was increased in the mPFC of LAP Tg mice, while significantly decreased in that of C/EBPβ knockdown mice with or without AAV-Dnm1l injection (Supplementary Fig. 7e). These results demonstrated the binding of C/EBPβ to the *Dnm1l* promoter gene is similar under different conditions in vivo. Together, these data

demonstrate that C/EBPβ enhances DRP1 expression in mPFC neurons and contributes to depressive-like effects in adolescent mice.

Different patterns of maternal separation trigger different outcomes in stress susceptibility via IGF-1-mediated C/EBPβ activity

In Figs. 1–4, we focus on adolescent stressors and mitochondrial function with adolescent chronic social defeat paradigm and

Fig. 3 | Neuronal C/EBPβ acts as a transcription activator for *Dnm1l* gene.
a Binding score of transcription factors bound to the *Dnm1l* promoter region determined by ChIP assays (ChIP-Atlas MACS2) in HeLa S3 cells obtained from the Signaling Pathway Project. **b** Measurement of mRNA levels of *Gabpa*, *Ctcf*, *Rest*, *Cebpb* in the control and susceptible mice. Data are presented the mean ± SEM (*n* = 6 for each group; two-sided unpaired *t*-test with Welch's correction). **c** Correlation analysis between social interaction ratio and relative *Cebpb* mRNA levels in WT mice exposed to AcSD or control. The white, red, and blue dots represent the control, susceptible, and resilient groups, respectively. The Spearman correlation coefficient *r*² and two-sided *p* value are shown (*n* = 6 for each group). **d** Representative immunoblots of p-C/EBPβ and C/EBPβ protein levels in the mPFC of WT mice exposed to AcSD or control. Data are representative of three independent experiments. **e** The immunostaining of p-C/EBPβ (Red) with *Dnm1l* mRNA (Green) in situ hybridization on the mPFC sections of WT mice exposed to AcSD or control. Scale bar: 10 μm. Correlation analysis between relative p-C/EBPβ intensity and social interaction ratio (**f**), or relative *Dnm1l* mRNA intensity (**g**) in WT mice exposed to AcSD or control. The white, red, and blue dots represent the control, susceptible, and resilient groups, respectively. The Spearman correlation coefficient *r*² and two-sided *p* value are shown (*n* = 8 for each group). **h** Immunofluorescence co-staining of C/EBPβ (green) and DRP1 (Red) on the brain sections of the mPFC in WT mice exposed to AcSD or control. Scale bars: 20 μm. **i** Quantification of C/EBPβ intensity in the mPFC from WT mice exposed to AcSD or control. Data are presented the mean ± SEM (*n* = 8 for each group; one-way ANOVA and Bonferroni's multiple comparison test). **j** Correlation analysis between relative DRP1 intensity and relative C/EBPβ intensity in WT mice exposed to AcSD or control. The white, red, and blue dots represent the control, susceptible, and resilient groups, respectively. The Spearman correlation coefficient *r*² and two-sided *p* value are shown (*n* = 8 for each group). **k** Snapshots of C/EBPβ ChIP-Seq at locus of *Dnm1l* gene in HeLa cells, HepG2 cells, HCT116 cells and MSCs cells. **l** Luciferase assays with different truncates of *Dnm1l* promoter in HEK293 cells co-transfected with GST or GST-C/EBPβ. Data are presented the mean ± SEM (*n* = 6 for each group; one-way ANOVA and Bonferroni's multiple comparison test). **m** Representative immunoblots of C/EBPβ protein expressions in HEK293 cells co-transfected with variants lengths of *Dnm1l* promoter and GST-C/EBPβ. Data are representative of three

independent experiments. **n** Luciferase assays with different truncates of *Dnm1l* promoter and representative immunoblotting bands of C/EBPβ protein expressions in HEK293 cells co-transfected with different truncates of *Dnm1l* promoter and si-control or si-C/EBPβ. Data are representative of three independent experiments. Data are presented the mean ± SEM (*n* = 5 for each group; one-way ANOVA and Bonferroni's multiple comparison test). **o** The consensus C/EBPβ-binding motif and sequence comparison of human and mouse *Dnm1l* promoters. **p** EMSA assay demonstrates that C/EBPβ binds the *Dnm1l* promoter. Nuclear extract proteins (NE) are isolated from HEK293 cells transfected with GST-C/EBPβ for 48 h. EMSA assay is recruited to detect the C/EBPβ binding ability on site −1369 to −1060 of *Dnm1l* promoter with probe (GTGGCGCAATC), mutation probe (GTGTATCAATC). Data are representative of three independent experiments. Probe bands indicate probe without binding of C/EBPβ protein. Shift bands indicate the C/EBPβ protein−Probe complex. Super-shift band indicates the C/EBPβ antibody−C/EBPβ protein−Probe complex. **q** ChIP-PCR assays demonstrate C/EBPβ specifically binds to *Dnm1l* promoter binding motif of genomic DNA. The C/EBPβ−DNA crosslinking ChIP samples are obtained from HEK293 cells and immunoprecipitated with anti-C/EBPβ or IgG antibodies. After reversing crosslinks, PCR are performed by using primer pairs at −1404 to −1195 of *Dnm1l* promoter. PCR assay also include each input sample. The positive control is demonstrated with anti-Histone H3 antibody coupling with GAPDH primers. Data are representative of three independent experiments. **r**, **s** Representative immunoblots and quantification of human and mouse C/EBPβ and DRP1 protein expressions in primary mouse neurons. Data are representative of three independent experiments. Data are presented the mean ± SEM (*n* = 5 for each group; one-way ANOVA and Bonferroni's multiple comparison test). **t** Measurement of *Dnm1l* mRNA levels in primary mouse neurons. Data are presented the mean ± SEM (*n* = 6 for each group; one-way ANOVA and Bonferroni's multiple comparison test). **u** Immunofluorescence co-staining of C/EBPβ (green) and DRP1 (Red) in primary mouse neurons. Scale bars: 10 μm. Quantification of C/EBPβ intensity (**v**) and DRP1 intensity (**w**) in primary mouse neurons. Data in (**v**) are presented the mean ± SEM (*n* = 10 for each group; ND not detected; two-sided unpaired *t*-test with Welch's correction). Data in (**w**) are presented the mean ± SEM (*n* = 10 for each group; one-way ANOVA and Bonferroni's multiple comparison test). See also Supplementary Fig. 6. Source data are provided as a Source Data file.

demonstrate that hyperactivation of C/EBPβ promotes stress susceptibility in adolescent mice, but the upstream mechanisms of C/EBPβ activation remain elusive. Given that C/EBPβ is an inflammation-related transcription factor[41,42], we have further investigated IL-6 and TNF-α levels in the mPFC of adolescent mice exposed to AcSD. Our results showed that only IL-6 level increased in the mPFC of susceptible adolescent mice (Supplementary Fig. 7f). However, blockade of IL-6 did not effectively inhibit neuronal C/EBPβ activity in the mPFC neurons of adolescent susceptible mice (Supplementary Fig. 7g, h)[43]. Thus, there may be another upstream mediating neuronal C/EBPβ activity in the adolescent susceptibility.
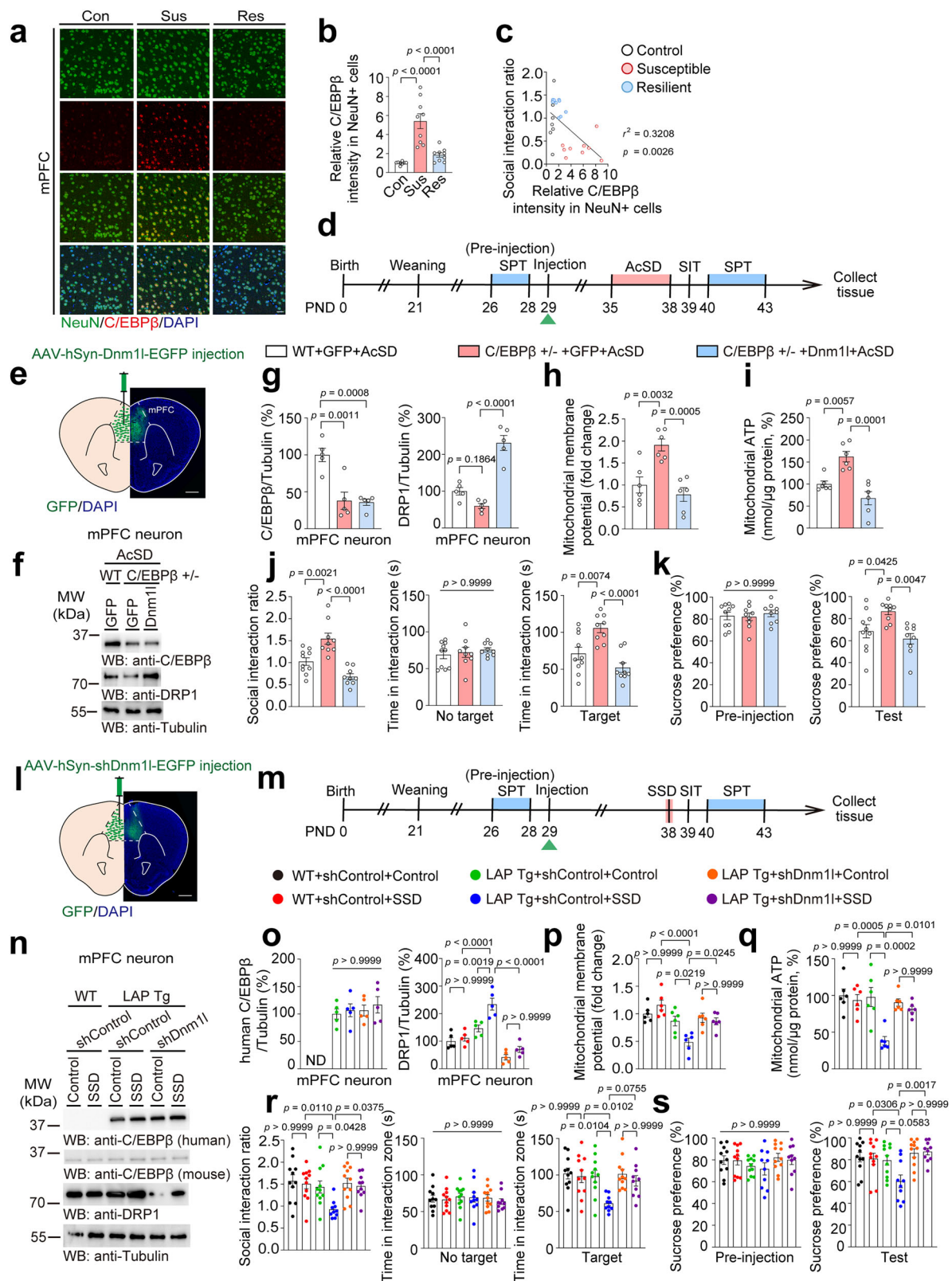
It is necessary to investigate this upstream signaling pathway because transcription factors are conventionally thought not to be pharmacological targets due to their mode of action and diverse physiological effects[44] and the upstream regulators of transcription factors are more "druggable" and worth to be investigated. Elucidating the upstream mechanisms driving C/EBPβ activation may provide preclinical evidence for the treatment of adolescent depression.

Epidemiological and preclinical studies suggest that adolescents' resilience to stressful events later in life is affected by severe early life stressors such as an unfavorable postnatal environment[12–15]. Thus, the "two-hit" model provides valuable insights into the upstream mechanisms that influence stress susceptibility in adolescents (Fig. 5a). Maternal separation (MS), a classic paradigm in the "two-hit" hypothesis, has been shown to modulate adolescent stress susceptibility (Supplementary Fig. 8a–g)[45,46]. Therefore, we switch from adolescent chronic social defeat to maternal separation, to investigate the upstream signaling pathway that promote neuronal C/EBPβ activity in adolescent mice exhibiting depressive-like behaviors.

Our results show that MS alters adolescent mPFC neuronal C/EBPβ activity and C/EBPβ LAP/LIP ratio (Fig. 5b–f, Supplementary

Fig. 8h). Consistent with this finding, we observed that C/EBPβ LAP/LIP ratio is increased in the mPFC of adolescent stress-susceptible mice with no postnatal stress (Supplementary Fig. 8i). These results suggest that the LAP/LIP ratio may be involved in the activation of C/EBPβ in adolescent depression, and further indicate that this ratio may play a role in the modulation of adolescent depression by early-life events. Previous studies have shown that the C/EBPβ LAP/LIP ratio is primarily modulated by mTORC1[39], which is regulated by IGF-1[47]. Thus, IGF-1 may regulate the C/EBPβ LAP/LIP ratio through IGF-1R/mTORC1 signaling pathway (Fig. 5g). Importantly, low IGF-1 levels have been detected in the brains of MS-exposed adolescents[48] and in the mPFC of adolescent stress-susceptible mice with no MS experience (Supplementary Fig. 8j). These results indicate that IGF-1 might be a "consistent regulator" under both MS and adolescent stress conditions, linking the two stressors in the different timelines.

Next, based on previous studies, we proposed an IGF-1-induced pathway (Fig. 5h). To test this hypothesis, we treated IGF-1 to primary mouse cortical neurons and found that IGF-1 treatment increased the phosphorylation of the IGF-1 receptor (IGF-1R), Akt and S6 kinase 1 (S6K1) in relation to the total ratio (Fig. 5i, Supplementary Fig. 8k). Importantly, this signaling cascade was associated with a reduced LAP/LIP ratio, suggesting that IGF-1, binding its receptor, activates mTORC1 signaling to suppress the LAP/LIP ratio (Fig. 5i, Supplementary Fig. 8k). Furthermore, although IGF-1 downregulated C/EBPβ activity, it did not alter total protein or mRNA levels of C/EBPβ (Supplementary Fig. 8l, k, 8m). This modulation of C/EBPβ activity coincided with a decrease in *Dnm1l* mRNA levels, which could be due to a competitive inhibitory effect exerted by the LIP isoform (Supplementary Fig. 8m). These results suggest that IGF-1 binding to its receptor activates mTORC1 signaling, leading to a decrease in the LAP/LIP ratio and thus affecting the neuronal stress susceptibility pathway.

Subsequently, to explore the role of IGF-1 in stress susceptibility in adolescent mice, we used a protocol of 10 min × 2 MS and AcSD with simultaneous injections of anti-IGF-1 or anti-IgG to block brain IGF-1 levels (Fig. 5j). The placement of cannula was shown in Supplementary Fig. 8n. The results showed that anti-IGF-1 restored the neuronal LAP/LIP ratio as well as the mRNA and protein levels of DRP1 compared to anti-IgG, while anti-IGF-1 reduced the social interaction ratio, time

spent in the interaction zone, and sucrose preference in stressed adolescent mice (Fig. 5k–m, Supplementary Fig. 8o–q). To assess the individual versus additive effects of stress, we performed the experiments with more groups (Supplementary Fig. 9a). The placement of cannula was shown in Supplementary Fig. 9b. The groups include no MS+Control+Anti-IgG, no MS+Control+Anti-IGF-1, no MS+AcSD+Anti-IgG, no MS+AcSD+Anti-IGF-1, 10 × 2 MS+Control+Anti-IgG, 10 × 2 MS+

Fig. 4 | Neuronal C/EBPβ acts as a transcription activator for *Dnm1l* and regulates stress susceptibility in adolescent mice. a Immunofluorescence co-staining of NeuN (green) and C/EBPβ (Red) on the brain sections of the mPFC in WT mice exposed to AcSD or control. Scale bars: 20 μm. **b** Quantification of C/EBPβ intensity in NeuN+ cells on the brain sections of the mPFC in WT mice exposed to AcSD or control. **c** Correlation analysis between social interaction ratio and C/EBPβ intensity in NeuN+ cells in WT mice exposed to AcSD or control. The white, red, and blue dots represent the control, susceptible, and resilient groups, respectively. The Spearman correlation coefficient r^2 and p value are shown. Data in (**b**, **c**) are presented the mean ± SEM ($n = 8$ for control group, $n = 9$ for susceptible group, $n = 9$ for resilient group; one-way ANOVA and Bonferroni's multiple comparison test). **d** Schematic representation of the experimental procedure for AcSD paradigm and behavioral test process for WT or C/EBPβ+/- mice, with virus injection of AAV-hSyn-EGFP or AAV-hSyn-Dnm1l-EGFP. **e** The location of the cannula tips and fluorescence microscopy image of representative field showed GFP expression in the mPFC injected with AAV-hSyn-Dnm1l-EGFP. Scale bar: 500 μm. $n = 3$ mice for each group. **f, g** Representative immunoblots and quantification of C/EBPβ and DRP1 protein expressions in the mPFC neurons of WT and C/EBPβ+/- mice with indicative treatments. Data are representative of three independent experiments. Data are presented the mean ± SEM ($n = 5$ for each group; one-way ANOVA and Bonferroni's multiple comparison test). Measurement of mitochondrial MMP (**h**) and ATP levels (**i**) in the mPFC of WT and C/EBPβ+/- mice with indicative treatments. Data in (**h**, **i**) are presented the mean ± SEM ($n = 6$ for each group; one-way ANOVA and Bonferroni's multiple comparison test). **j, k** Behavioral tests of WT and C/EBPβ+/- mice exposed to AcSD paradigm with virus injection of AAV-hSyn-EGFP or AAV-hSyn-shDnm1l-EGFP. Measurement of social interaction ratio, time in interaction zone without or with target (**j**), and the percentage of sucrose preference (**k**) in WT and

C/EBPβ+/- mice with indicative treatments. Data in (**j**, **k**) are presented as the mean ± SEM ($n = 10$ mice for WT + GFP + AcSD group; $n = 9$ mice for C/EBPβ +/- + GFP + AcSD group; $n = 9$ mice for C/EBPβ+/- + Dnm1l + AcSD group; one-way ANOVA and Bonferroni's multiple comparison test). **l** The location of the cannula tips and fluorescence microscopy image of representative field showed GFP expression in the mPFC injected with AAV-hSyn-shDnm1l-EGFP. Scale bar: 500 μm. $n = 3$ mice for each group. **m** Schematic representation of the experimental procedure for SSD paradigm and behavioral test process for WT or LAP Tg mice, with virus injection of AAV-hSyn-EGFP or AAV-hSyn-shDnm1l-EGFP. **n, o** Representative immunoblots and quantification of human and mouse C/EBPβ and DRP1 protein expressions in the mPFC neurons of WT and LAP Tg mice with indicative treatments. Data are representative of three independent experiments. Data are presented the mean ± SEM ($n = 5$ for each group; ND, not detected; one-way ANOVA and Bonferroni's multiple comparison test). Measurement of mitochondrial MMP (**p**) and ATP levels (**q**) in the mPFC of WT and LAP Tg mice with indicative treatments. Data in (**p**, **q**) are presented the mean ± SEM ($n = 6$ for each group; one-way ANOVA and Bonferroni's multiple comparison test). **r, s** Behavioral tests of WT and LAP Tg mice exposed to SSD paradigm with virus injection of AAV-hSyn-shControl-EGFP or AAV-hSyn-shDnm1l-EGFP. Measurement of social interaction ratio, time in interaction zone without or with target (**r**), and the percentage of sucrose preference (**s**) in WT and LAP Tg mice with indicative treatments. Data in (**r**, **s**) are presented as the mean ± SEM ($n = 11$ mice for WT + shControl + Control group, $n = 11$ mice for WT + shControl + SSD group, $n = 11$ mice for LAP Tg + shControl + Control group, $n = 10$ mice for LAP Tg + shControl + SSD group, $n = 11$ mice for LAP Tg + shDnm1l + Control group, $n = 10$ mice for LAP Tg + shDnm1l + SSD group; one-way ANOVA and Bonferroni's multiple comparison test). See also Supplementary Fig. 7. Source data are provided as a Source Data file.

Control+Anti-IGF-1, 10 × 2 MS+AcSD+Anti-IgG, 10 × 2 MS+AcSD+Anti-IGF-1. The results showed that anti-IGF-1 antibody alone or AcSD alone promoted mPFC neuronal C/EBPβ/DRP1 signaling pathway, and induced social avoidance and sucrose preference deficits in adolescent mice (Supplementary Fig. 9c–f). These changes were exacerbated by the additive effects of anti-IGF-1 antibody and AcSD (Supplementary Fig. 9c–f). However, 10 min × 2 MS suppressed C/EBPβ/DRP1 axis and restored behavioral performance in adolescent mice received anti-IGF-1 antibody treatment or AcSD or both them (Supplementary Fig. 9c–f). This suggests that 10 min × 2 MS-induced upregulation of IGF-1 is important for maintaining stress resilience in adolescent mice. In addition, after screening susceptible adolescent mice by social interaction test, we treated them with IGF-1 or vehicle, and found that IGF-1 reduced LAP/LIP ratio and DRP1 protein expression in MS-free adolescent mice (Fig. 5n–p, Supplementary Fig. 10i, j). IGF-1 treatment also ameliorated social avoidance and sucrose preference deficits in these mice (Fig. 5q, r, Supplementary Fig. 10k). Furthermore, prolonged IGF-1 treatment in adolescent mice undergoing 180 min MS reversed the increased LAP/LIP ratio and C/EBPβ activity, and subsequently reduced DRP1 mRNA and protein levels, significantly alleviating social avoidance and depressive-like behaviors (Supplementary Fig. 10a–h). These results highlight that brain-specific IGF-1 is a key molecular mediator in mediating stress vulnerability in adolescent mice experiencing MS and social defeat, and C/EBPβ-DRP1 axis is an important downstream pathway through modulation of the LAP/LIP ratio (Supplementary Fig. 10l).

Maternal behavior protects against stress vulnerability via upregulating mPFC IGF-1 levels in adolescent mice
MS might lead to changes in maternal behavior. To further understand the reason why different MS leads to different outcomes, we quantified maternal behaviors, such as nursing postures (NP), licking/grooming, and nest building for MS (Fig. 6a). The results showed that maternal behavior sample points increased in the 10 min × 2-MS group but decreased in the 180 min × 1-MS group compared to the control group (Fig. 6a). In addition, maternal behavior sample points were positively correlated with both social interaction ratios and mPFC IGF-1 levels, suggesting that maternal care is an important mediator of MS-induced

social avoidance and IGF-1 downregulation (Fig. 6b, c). Notably, there was also a positive correlation between mPFC IGF-1 levels and social interaction ratios (Fig. 6d). These findings suggest that maternal behavior is important in regulating mPFC IGF-1 levels and protecting adolescent mice from stress susceptibility.

To further elucidate the relationship between maternal behaviors and stress susceptibility in adolescent mice, we employed LnL (Lactating, and non-Lactating mothers) model to increase maternal behaviors for pups, and conducted 180 min × 1 MS and following AcSD paradigm (Fig. 6e)[49]. The results showed that the sample points of maternal behavior in the LnL group were higher than those in the L group in both the 180 min × 1 MS and control conditions, suggesting that the LnL model was effective in enhancing maternal care (Fig. 6f). Besides, increased maternal care induced elevated IGF-1 levels in the mPFC, but not in the hippocampus or blood, suggesting that local IGF-1 levels in the mPFC are regulated by maternal behaviors (Fig. 6g). Further, we isolated mPFC from pups and found that LnL decreased LAP/LIP ratio and DRP1 protein expression, as well as *Dnm1l* mRNA levels, suggesting that increased maternal care induced elevated IGF-1 levels in the mPFC and suppressed the C/EBPβ-DRP1 axis (Fig. 6h, Supplementary Fig. 11a, b). Consistently, long MS-induced social avoidance and sucrose preference deficits were ameliorated by LnL, resulting from decreased C/EBPβ/DRP1-mediated mitochondrial dysfunction (Fig. 6i, j, Supplementary Fig. 11c). Additionally, compared with those in the L group, the pups in the LnL groups did not show obvious changes on the body weight during the experimental process, indicating the improved maternal care did not result in better nurture (Supplementary Fig. 11d).

Next, we asked whether IGF-1 is responsible for the antidepressant role of maternal behavior in LnL-treated offspring, we injected either an anti-IGF-1 antibody or an anti-IgG antibody into adolescent mice treated with LnL (Supplementary Fig. 12a). The placement of cannula was shown in Supplementary Fig. 12b. Although neither treatment affected maternal behavior, blockade of IGF-1 increased the LAP/LIP ratio, which in turn increased DRP1 mRNA and protein levels, suggesting that IGF-1 is important for inhibiting the role of the C/EBPβ-DRP1 axis in AcSD-induced stress susceptibility in adolescents (Supplementary Fig. 12c–e). Behavior tests showed that mice receiving the
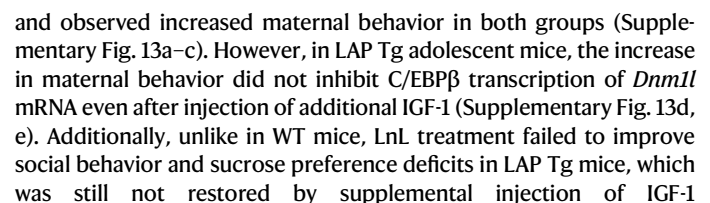
anti-IGF-1 antibody exhibited social avoidance, reduced time in interaction zone and deficits in sucrose preference, suggesting blocking IGF-1 diminished the protective effects of LnL against AcSD-induced stress susceptibility (Supplementary Fig. 12f, g). These results indicate that maternal behavior upregulates IGF-1 levels to inhibit C/EBPβ activity, thereby bolstering stress resilience in adolescent mice under stress. Furthermore, we treated both WT and LAP Tg mice with LnL,

and observed increased maternal behavior in both groups (Supplementary Fig. 13a–c). However, in LAP Tg adolescent mice, the increase in maternal behavior did not inhibit C/EBPβ transcription of *Dnm1l* mRNA even after injection of additional IGF-1 (Supplementary Fig. 13d, e). Additionally, unlike in WT mice, LnL treatment failed to improve social behavior and sucrose preference deficits in LAP Tg mice, which was still not restored by supplemental injection of IGF-1

Fig. 5 | Different patterns of maternal separation trigger different outcomes in stress susceptibility via IGF-1-mediated C/EBPβ activity. a Schematic representation of the upstream signaling pathway of early life experience affecting C/EBPβ/DRP1 axis, contributing to adolescent depression. **b** Schematic representation of the experimental procedure for maternal separation on different durations, and AcSD paradigm. **c** Measurement of C/EBPβ activity in the mPFC neurons of WT mice exposed to different maternal separations and AcSD. **d** Measurement of *Cebpb* mRNA levels in the mPFC neurons of WT mice exposed to different maternal separations and AcSD. Data in (**c, d**) are presented as the mean ± SEM ($n = 4$ for each group; one-way ANOVA and Bonferroni's multiple comparison test). **e, f.** Representative immunoblots and quantification of LAP/LIP ratio in the mPFC neurons of WT mice from (**b**). Data are representative of three independent experiments. Data are presented the mean ± SEM ($n = 4$ for each group; one-way ANOVA and Bonferroni's multiple comparison test). **g** Schematic representation of molecular pathway hypothesis that IGF-1 induces inhibition of neuronal C/EBPβ activity. **h** Measurement of the IGF-1 levels in the blood, the mPFC and the hippocampus of WT mice from (**b**). Data are presented the mean ± SEM ($n = 6$ for each group; one-way ANOVA and Bonferroni's multiple comparison test). **i** Representative immunoblots of LAP/LIP ratio, p-IGF-1R/IGF-1R, p-Akt/Akt and p-S6K1/S6K1 in the primary mouse cortex neurons with vehicle or IGF-1. Data are representative of three independent experiments. **j** Schematic representation of the experimental procedure for maternal separation for 10 min × 2, and AcSD paradigm and behavioral tests with the mPFC infusion of anti-IgG or anti-IGF-1. **k** Representative immunoblots of LAP/LIP ratio and DRP1 expressions in the mPFC neurons of WT mice exposed to maternal separation for 10 min × 2, and AcSD paradigm with the mPFC

infusion of anti-IgG or anti-IGF-1. Data are representative of three independent experiments. **l, m** Behavioral tests of WT mice exposed to maternal separation for 10 min × 2, and AcSD paradigm with the mPFC infusion of anti-IgG or anti-IGF-1. Measurement of social interaction ratio, time in interaction zone with target (**l**), and the percentage of sucrose preference (**m**) in WT mice with indicative treatments. Data in (**l, m**) are presented as the mean ± SEM ($n = 8$ mice for anti-IgG group, $n = 10$ mice for anti-IGF-1 group; unpaired *t*-test with Welch's correction). **n** Schematic representation of the experimental procedure for AcSD paradigm and behavioral tests with the mPFC infusion of vehicle or IGF-1. **o** Representative immunoblots and quantification of LAP/LIP ratio, and p-DRP1 and DRP1 expressions in the mPFC neurons of WT susceptible mice exposed to AcSD paradigm with the mPFC infusion of vehicle or IGF-1. Data are representative of three independent experiments. Data in (**o**) are presented as the mean ± SEM ($n = 6$ for each group; two-sided unpaired *t*-test with Welch's correction). **p** Scatter plot depicting the distribution of social interaction ratio for susceptible (ratio < 1), and resilient (ratio ≥ 1) after the AcSD paradigm. The red, and blue dots represent the susceptible, and resilient groups, respectively. Data in (**p**) are presented as the mean ± SEM ($n = 22$ for susceptible group; $n = 26$ for resilient group; two-sided unpaired *t*-test with Welch's correction). **q, r** Behavioral tests of WT susceptible mice exposed to AcSD paradigm with the mPFC infusion of vehicle or IGF-1. Measurement of social interaction ratio, time in interaction zone with target (**q**), and the percentage of sucrose preference (**r**) in WT susceptible mice with indicative treatments. Data in (**q, r**) are presented as the mean ± SEM ($n = 9$ mice for each group; two-sided unpaired *t*-test with Welch's correction). See also Supplementary Figs. 8–10. Source data are provided as a Source Data file.

(Supplementary Fig. 13f, g). These results show that maternal behavior-elevated IGF-1 levels prevents stress susceptibility through modulation of LAP/LIP ratio.
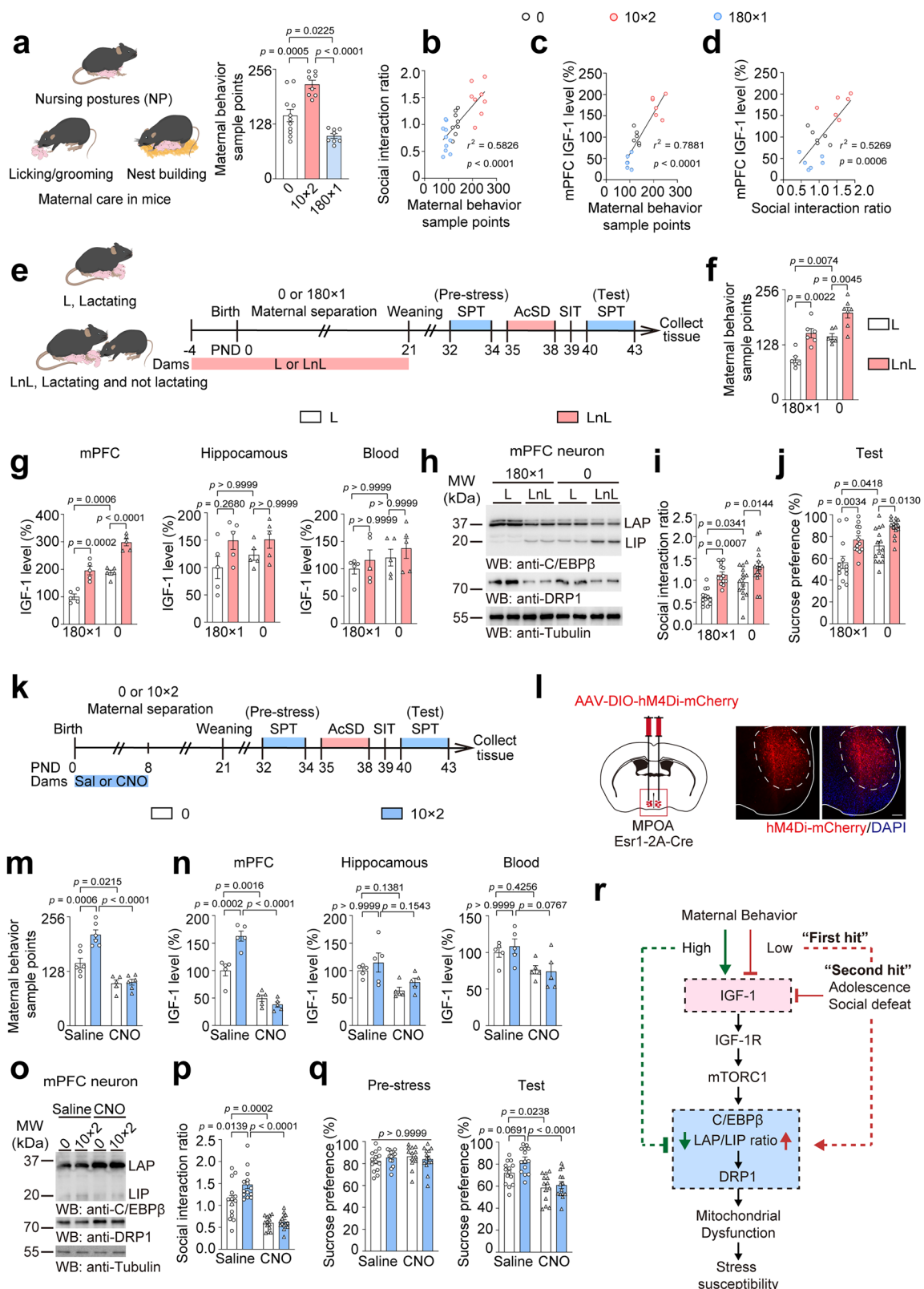
The medial preoptic area (MPOA) has been reported to be an important brain region for maternal behavior, and in particularly Esr1+ cells in MPOA are naturally and preferentially activated during maternal behaviors[50–53]. To further explain the relationship between maternal care in early period and stress susceptibility in adolescence, we utilized chemogenetic method to abolish the activities of MPOA^Esr1+ cells of dams at PND 0–8, in order to decrease maternal behavior in early period, and performed 10 min × 2 MS or control and following AcSD paradigm (Fig. 6k, l). CNO-treated dams exhibited reduced maternal behaviors sample points for both 10 min × 2 MS and control pups, compared with saline-treated dams which showed increased maternal behavior sample points in 10 min × 2 MS (Fig. 6m). Similarly, CNO treatment in dams reduced the IGF-1 levels in the mPFC of both 10 min × 2 MS and control pups, whereas IGF-1 levels in the hippocampus or blood of pups were unchanged (Fig. 6n). Further analysis of the pups' mPFC revealed an increased LAP/LIP ratio and elevated mRNA and protein levels of DRP1, which were associated with maternal behavioral deficits (Fig. 6o, Supplementary Fig. 14a, b). Behavior assessments indicated that the reduction in maternal behaviors led to social avoidance and sucrose preference deficits in adolescent offspring, suggesting the lack of early maternal behavior contributes to stress susceptibility during adolescence (Fig. 6p, q, Supplementary Fig. 14c). Additionally, compared with the pups with saline-treated dams, those with CNO-treated dams displayed no changes on the body weight until PND 21, suggesting the decreased maternal behavior did not lead to poor nurture (Supplementary Fig. 14d).

Furthermore, we supplemented pups lacking early maternal behavior with IGF-1 during puberty (Supplementary Fig. 15a–d). The results showed that IGF-1 supplementation reduced *Dnm1l* mRNA levels in WT pups, suggesting that maternal behavior suppresses the C/EBPβ-DRP1 axis mainly through IGF-1 levels. However, this suppression of *Dnm1l* mRNA was not observed in LAP Tg pups, indicating that the LAP/LIP ratio is a key downstream of maternal behavior-mediated IGF-1 (Supplementary Fig. 15e, f). Consistently, IGF-1 supplement improved social behavior and sucrose preference in WT mice, but not in LAP Tg mice (Supplementary Fig. 15g, h). In addition, *Dnm1l* mRNA levels were not increased in C/EBPβ+/- pups despite the absence of maternal

behavior early in life (Supplementary Fig. 16a–e). Consequently, as a result of reduced C/EBPβ activity, C/EBPβ+/- pups showed increased social interaction ratios, longer interaction times, and stronger sucrose preference in behavioral tests, suggesting that inactivation of the C/EBPβ-DRP1 axis improves stress resilience in adolescent mice (Supplementary Fig. 16f, g). Overall, these results suggest that early maternal behavior in young mice is important for fostering stress resilience and preventing depressive-like behaviors by regulating mPFC IGF-1 levels during puberty (Fig. 6r).

Microglial-derived IGF-1 inhibits neuronal C/EBPβ-DRP1 axis to prevent stress susceptibility in adolescent mice

The above data suggest that maternal behavior-stimulated IGF-1 inhibit the C/EBPβ-DRP1 axis in the mPFC neurons, thereby preventing stress susceptibility in adolescent mice. To further elucidate the source of maternal care-induced IGF-1, we performed two experiments: in the first experiment pups were treated with L or LnL, and in the second experiment dams were treated with saline or CNO, and assessed IGF-1 levels in the unstressed pups of both experiments (Fig. 7a). Immunostaining confirmed hM4Di expression in the second experiment (Fig. 7b). Consistent with our previous findings, maternal behavior sample points increased in the LnL group and decreased in the CNO-treated group (Fig. 7c). In addition, IGF-1 levels in the mPFC were positively correlated with changes in maternal behavior, whereas IGF-1 levels in blood or hippocampus were not (Fig. 7d, Supplementary Fig. 17a, b). Given that IGF-1 can act through autocrine or paracrine mechanisms[54], we measured the mRNA levels of *Igf1* in the mPFC and found that *Igf1* mRNA levels were correlated with maternal behavior tendencies, suggesting increased IGF-1 levels might be due to local protein synthesis (Fig. 7e). To identify the cell type primarily responsible for maternal behavior-mediated IGF-1 synthesis, we stained *Igf1* mRNA with neuronal marker (NeuN), but there was no significant co-localization between *Igf1* mRNA and NeuN intensities in the mPFC, irrespective of maternal care levels (Supplementary Fig. 17c, d). Further analysis showed that *Igf1* mRNA levels in NeuN+ cells were similar in pups, whereas *Igf1* mRNA levels in NeuN- cells varied according to maternal behavioral tendencies, suggesting non-neuronal cells such as glial cells might be the primary source for maternal behavior-mediated IGF-1 synthesis (Supplementary Fig. 17e, f). Subsequent co-immunostaining with microglial marker (Iba1) revealed high

colocalization with *Igf1* mRNA, consistent with the observation that microglia are the major source of IGF-1 in the early period of pups (Fig. 7f, g)[55]. Further analysis demonstrated that *Igf1* mRNA levels in Iba1+ cells increased in the LnL group but a decreased in the CNO-treated dams' group, with no difference in Iba1- cells among all groups (Fig. 7f, g). These results support that the microglia are the main source of IGF-1 in the mPFC of pups in response to maternal behavior.

Additionally, isolated CD11b+ cells (microglia) from the mPFC of PND 35 mice showed a corresponding increase or decrease, consistent with the immunostaining results (Supplementary Fig. 17g). Notably, maternal care-induced microglial IGF-1 elevation was present from the time of weaning at PND 21 until PND 35, which is accordance with those exposed to 10 min × 2 or 180 min × 1 MS, demonstrating the impact of maternal care was microglia-specific (Supplementary Fig. 17h, i). We

Fig. 6 | Maternal behavior protects against stress vulnerability via upregulating mPFC IGF-1 levels in adolescent mice. a Graphic representation of maternal behavior in mice; Measurement of maternal behavior sample points in WT mice exposed to maternal separation for 0, 10 min × 2, and 180 min × 1. Data are presented the mean ± SEM ($n = 11$ mice for no maternal separation group, $n = 8$ mice for maternal separation on 10 min × 2 group, $n = 8$ mice for maternal separation on 180 min × 1 group; one-way ANOVA and Bonferroni's multiple comparison test). **b** Correlation analysis between social interaction ratio and maternal behavior sample points in WT mice experiencing maternal separation. The white, red, and blue dots represent 0, 10 min × 2, and 180 min × 1 groups, respectively. The Spearman correlation coefficient r^2 and two-sided p value are shown ($n = 8$ mice for no maternal separation group, $n = 8$ mice for 10 min × 2 group, $n = 10$ mice for 180 min × 1 group). Correlation analysis between mPFC IGF-1 levels and maternal behavior sample points (**c**), or social interaction ratio (**d**) in WT mice experiencing maternal separation. The white, red, and blue dots represent 0, 10 min × 2, and 180 min × 1 groups, respectively. The Spearman correlation coefficient r^2 and two-sided p value are shown ($n = 6$ mice for each group). **e** Graphic representation of L and LnL treatment; Schematic representation of the experimental procedure for maternal separation on 180 min × 1 or not, and AcSD paradigm and behavioral tests with L or LnL dams. **f** Measurement of maternal behavior sample points in WT mice exposed to maternal separation for 180 min × 1 or 0, with L or LnL dams. Data are presented the mean ± SEM ($n = 6$ mice for 180 × 1 + L group, $n = 6$ mice for 180 × 1 + LnL group, $n = 6$ mice for 0 + L group; $n = 7$ mice for 0 + LnL group; one-way ANOVA and Bonferroni's multiple comparison test). **g** Measurement of IGF-1 levels in the mPFC, in the hippocampus, and in the blood in WT mice exposed to maternal separation for 180 min × 1 or 0, with L or LnL dams. Data are presented the mean ± SEM ($n = 5$ for each group; one-way ANOVA and Bonferroni's multiple comparison test). **h** Representative immunoblots of LAP/LIP ratio and DRP1 expressions in the mPFC neurons of WT mice exposed to maternal separation for 180 min × 1 or 0, with L or LnL dams. Data are representative of three independent experiments. **i, j** Behavioral tests of WT mice exposed to maternal separation for 180 min × 1 or 0, with L or LnL dams. Measurement of social interaction ratio (**i**), and the percentage of sucrose preference (**j**) in WT mice with indicative treatments. Data in (**i, j**) are presented as the mean ± SEM ($n = 13$ mice for 180 × 1 groups, $n = 15$ mice for 0 groups; one-way ANOVA and Bonferroni's multiple comparison test). **k** Schematic representation of the experimental procedure for maternal separation on 10 min × 2 or not, and AcSD paradigm and behavioral tests with saline- or CNO-treated dams. **l** The location of the cannula tips in Esr-2A-Cre female mice; Fluorescence microscopy image of representative field showed mCherry expression in the MPOA injected with AAV-DIO-hM4Di-mCherry. Scale bar: 100 μm. $n = 4$ dams for each group. **m** Measurement of maternal behavior sample points in WT mice exposed to maternal separation for 10 min × 2 or 0, with saline- or CNO-treated dams. Data are presented the mean ± SEM ($n = 6$ mice for 0 + Saline group, $n = 6$ mice for 10 × 2 + Saline group, $n = 5$ mice for 0 + CNO group; $n = 6$ mice for 10 × 2 + CNO group; one-way ANOVA and Bonferroni's multiple comparison test). **n** Measurement of IGF-1 levels in the mPFC, in the hippocampus, and in the blood in WT mice exposed to maternal separation for 10 min × 2 or 0, with saline- or CNO-treated dams. Data are presented the mean ± SEM ($n = 5$ for each group; one-way ANOVA and Bonferroni's multiple comparison test). **o** Representative immunoblots of LAP/LIP ratio and DRP1 expressions in mPFC neurons of WT mice exposed to maternal separation for 10 min × 2 or 0, with saline- or CNO-treated dams. Data are representative of three independent experiments. **p, q** Behavioral tests of WT mice exposed to maternal separation for 10 min × 2 or 0, with saline- or CNO-treated dams. Measurement of social interaction ratio (**p**), and the percentage of sucrose preference (**q**) in WT mice with indicative treatments. Data in (**p, q**) are presented as the mean ± SEM ($n = 14$ mice for 0 + Saline group, $n = 14$ mice for 10 × 2 + Saline group, $n = 13$ mice for 0 + CNO group; $n = 14$ mice for 10 × 2 + CNO group; one-way ANOVA and Bonferroni's multiple comparison test). **r.** Schematic representation of molecular pathway that various maternal behavior levels mediate stress susceptibility via the "two-hit" hypothesis. See also Supplementary Figs. 11–16. Source data are provided as a Source Data file.
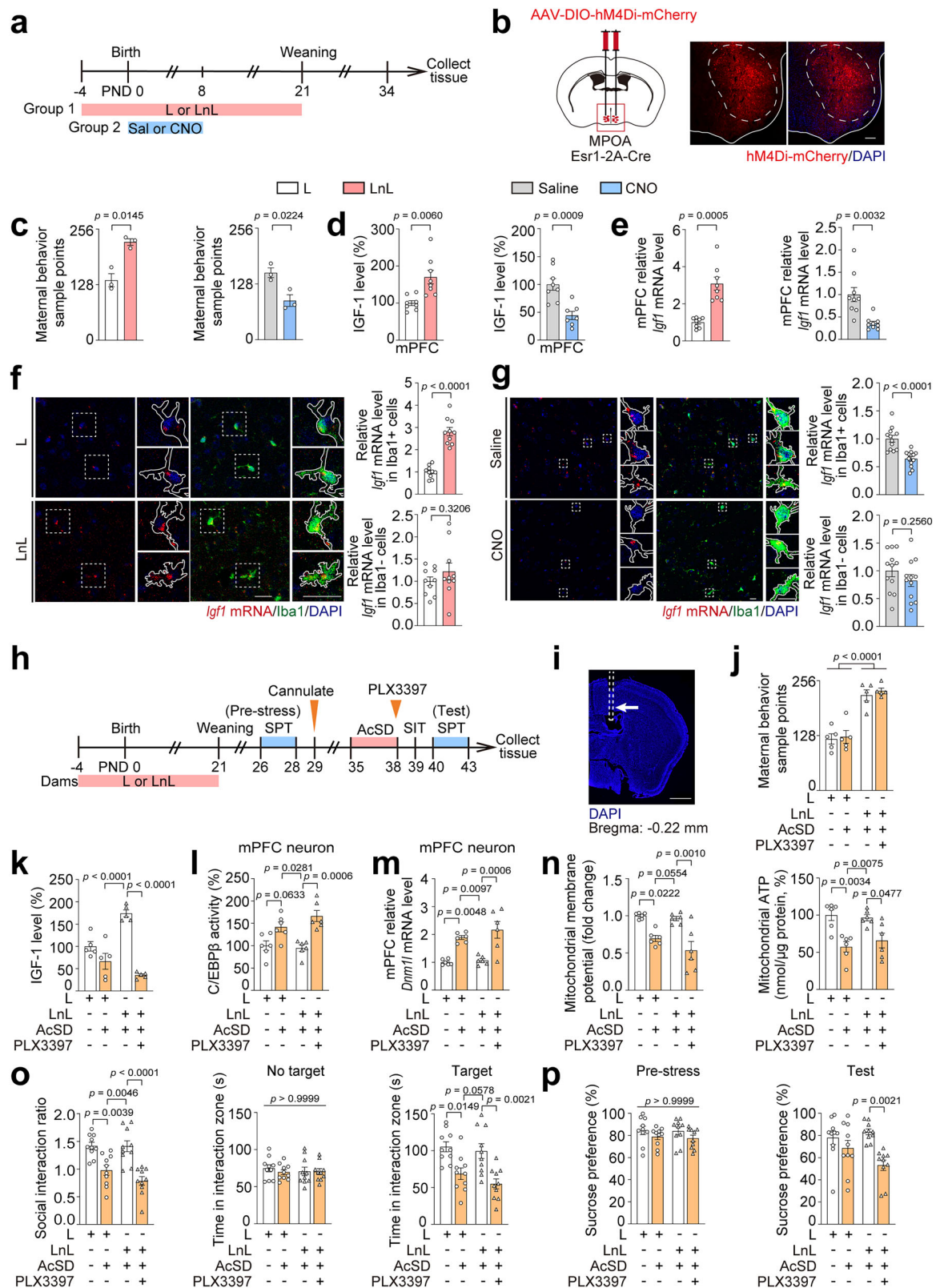
further tested the *Igf1* mRNA levels in microglia in the mPFC from the PND 60 mice (Supplementary Fig. 17h, i). The results showed that until PND 60, there was a sight but not significant increase in the level of IGF-1 in mice with LnL or exposed to 10 min × 2 MS (Supplementary Fig. 17h, i). Moreover, we examined microglial *Igf1* mRNA levels in the mPFC of mice exposed to 180 min × 1 MS which resulted in less maternal care, and the results showed mPFC microglial *Igf1* mRNA level was decreased in the offspring experiencing low maternal care at PND 60 (Supplementary Fig. 17i). Thus, our findings support that maternal care-induced IGF-1 microglial dysfunction persists into adulthood.

Microglia are the only cell type in the brain that expresses CSF1R, which is critical for microglia survival. Administration of the CSF1R inhibitor PLX3397 effectively depletes microglia[56]. To investigate the role of microglia in maternal behavior-mediated antidepressant-like effects of IGF-1 in adolescent mice, we administered PLX3397 to pups after L or LnL treatment and AcSD paradigm (Fig. 7h). The placement of cannula was shown in Fig. 7i. The results showed that PLX3397 treatment blocked LnL-induced IGF-1 elevation and C/EBPβ-DRP1 activation in the mPFC, consequently inducing DRP1-related mitochondrial dysfunction (Fig. 7j–n). These results suggest that microglia depletion diminishes IGF-1 levels, which then activates the C/EBPβ transcriptional activity for *Dnm1l*, leading to mitochondrial dysfunction. Behavior tests showed PLX3397 treatment abolished the protective effects of increased maternal behavior in response to AcSD, resulting in reduced social interaction, decreased time in the interaction zone, and impaired sucrose preference (Fig. 7o, p).

Activated microglia can be categorized into pro-inflammatory and anti-inflammatory phenotypes, with neurotoxic or neuroprotective effects in the brain. To further investigate the protective role of microglia in adolescent depressive-like behavior, we injected MCLs, an inhibitor of anti-inflammatory phenotype of microglia, into the mPFC of pups to decrease neuroprotective microglia expression (Supplementary Fig. 18a). The placement of cannula was shown in Supplementary Fig. 18b. Similar to PLX3397, MCLs treatment decreased the

IGF levels, and induced C/EBPβ activation and following *Dnm1l* mRNA levels in the LnL groups subjected to the AcSD paradigm (Supplementary Fig. 18c–f). Moreover, MCLs injection diminished the mitochondrial function improvements associated with increased maternal behavior, indicating that IGF-1 mainly originates from anti-inflammatory microglia (Supplementary Fig. 18g). Behavior test results confirmed the anti-depressive-like effects of anti-inflammatory microglia, with MCLs treatment leading to social avoidance and sucrose preference deficits (Supplementary Fig. 18h, i). Collectively, these results suggest that anti-inflammatory microglia in the mPFC are activated by maternal care to produce and secrete IGF-1, which prevents depressive-like behaviors by improving neuronal mitochondrial function in adolescent mice.

To gain insight into the interplay between microglia and neurons, we manipulated microglia-derived IGF-1 levels using Cx3cr1-Cre mice and AAV-MG1.2-DIO viruses[57–59], and overexpressed C/EBPβ isoforms specifically in neurons using AAV-hSyn viruses. First, we selectively inhibited microglia-derived IGF-1 levels and overexpressed the LIP isoform in LnL-treated pup mPFC neurons (Fig. 8a). The efficacy of viruses was validated through the immunostaining and the IGF-1 measurement in the mPFC (Fig. 8b, Supplementary Fig. 19a–c). Western blotting analysis further confirmed the virus expression and showed that microglial IGF-1 knockdown increased the LAP/LIP ratio and DRP1 protein expression, however, neuronal overexpression of the LIP isoform reversed this increase (Fig. 8c, d). Importantly, there were no differences in maternal behaviors of dams among all the groups (Fig. 8e). The increased DRP1 protein expression was attributed to upregulated *Dnm1l* mRNA levels, and promoted mitochondrial dysfunction, which was also diminished by LIP overexpression in neurons (Fig. 8f, g). Notably, depletion of microglia-derived IGF-1 induced social avoidance and sucrose preference deficits even under LnL conditions, yet neuronal LIP overexpression attenuated depressive-like behaviors in adolescent mice (Fig. 8h, i, Supplementary Fig. 19d).

On the other hand, we specifically supplemented IGF-1 in microglia and overexpressed the LAP isoform in neurons of the mPFC in pups with CNO-treated dams (Fig. 8j). Immunostaining and ELISA confirmed virus expression (Fig. 8k, Supplementary Fig. 19e–g). Western blot analysis demonstrated that supplementation of microglia with IGF-1 suppressed LAP/LIP ratios and thus reduced DRP1 protein expression, whereas overexpression of neuronal LAP restored these

reductions (Fig. 8l, m). The IGF-1 supplement and LAP overexpression did not impact maternal behaviors in dams (Fig. 8n). qPCR analysis revealed that *Dnm1l* mRNA levels were decreased by IGF-1 supplement in microglia, but increased by neuronal LAP overexpression (Fig. 8o). Similarly, mitochondrial MMP and ATP levels were upregulated by microglial IGF-1 supplement, but were impaired by neuronal LAP overexpression (Fig. 8p). Behavior tests results indicated that

Fig. 7 | Microglia are primary source of maternal behavior-mediated IGF-1 levels in the mPFC of adolescent mice. a Schematic representation of the experimental procedure for WT mice with L or LnL dams in group 1, and saline- or CNO-treated dams in group 2. **b** The location of the cannula tips in Esr-2A-Cre female mice; Fluorescence microscopy image of representative field showed mCherry expression in the MPOA injected with AAV-DIO-hM4Di-mCherry. Scale bar: 100 μm. $n = 3$ dams for each group. **c** Measurement of maternal behavior sample points in WT mice with L or LnL dams, and saline- or CNO-treated dams. Data are presented the mean ± SEM ($n = 3$ mice for each group; two-sided unpaired t-test with Welch's correction). **d** Measurement of IGF-1 levels in the mPFC of WT mice with L or LnL dams, and saline- or CNO-treated dams. Data are presented the mean ± SEM ($n = 8$ for L group; $n = 8$ for LnL group; $n = 8$ for Saline group; $n = 7$ for CNO group; two-sided unpaired t-test with Welch's correction). **e** Measurement of *Igf1* mRNA levels in the mPFC of WT mice with L or LnL dams, and saline- or CNO-treated dams. Data are presented the mean ± SEM ($n = 8$ for L or LnL group, $n = 9$ mice for Saline or CNO group; two-sided unpaired t-test with Welch's correction). The immunostaining of Iba1 (Green) with *Igf1* mRNA (Red) in situ hybridization on the mPFC sections of WT mice with L or LnL dams (**f**), and saline- or CNO-treated dams (**g**). Scale bar: 10 μm (**f**), 10 μm (**g**); Quantification of *Igf1* mRNA intensity in Iba1+ cells, and Iba1− cells. Data in (**f, g**) are presented the mean ± SEM ($n = 10$ for L or LnL group, $n = 12$ for Saline or CNO group; two-sided unpaired t-test with Welch's correction). **h** Schematic representation of the experimental procedure of PLX3397 treatment, and AcSD paradigm and behavioral tests for WT mice with L or LnL dams. **i** The image of cannula placements for injection of PLX3397. White arrow

indicates cannula target region and dotted line regions correspond to the position of the cannula. Bregma: −0.22 mm, Scale bar: 500 μm. $n = 3$ mice for each group. **j** Measurement of maternal behavior sample points in WT mice exposed to L or LnL dams, and AcSD paradigm with PLX3397 treatment. Data are presented the mean ± SEM ($n = 5$ mice for each group; one-way ANOVA and Bonferroni's multiple comparison test). **k** Measurement of IGF-1 levels in the mPFC from WT mice with indicative treatments. Data are presented the mean ± SEM ($n = 5$ for each group; one-way ANOVA and Bonferroni's multiple comparison test). **l** Measurement of C/EBPβ activity in the mPFC neurons from WT mice with indicative treatments. Data are presented the mean ± SEM ($n = 6$ for each group; one-way ANOVA and Bonferroni's multiple comparison test). **m** Measurement of *Dnm1l* mRNA levels in the mPFC neurons from WT mice with indicative treatments. Data are presented the mean ± SEM ($n = 6$ for each group; one-way ANOVA and Bonferroni's multiple comparison test). **n** Measurement of mitochondrial MMP and ATP levels in the mPFC of WT mice with indicative treatments. Data are presented the mean ± SEM ($n = 6$ for each group; one-way ANOVA and Bonferroni's multiple comparison test). **o, p** Behavioral tests of WT mice exposed to L or LnL dams, and AcSD paradigm with PLX3397 treatment. Measurement of social interaction ratio and time in interaction zone without or with target (**o**), and the percentage of sucrose preference (**p**) in WT mice with indicative treatments. Data in (**o, p**) are presented as the mean ± SEM ($n = 10$ mice for each group; one-way ANOVA and Bonferroni's multiple comparison test). See also Supplementary Figs. 17, 18. Source data are provided as a Source Data file.

microglial IGF-1 supplementation ameliorated social avoidance and sucrose preference deficits in response to social stress, which was reversed by neuronal LAP overexpression in pups under conditions of decreased maternal behavior (Fig. 8p, r, Supplementary Fig. 19h). Above all, these results highlight that microglia-to-neuron crosstalk plays an important role in mediating stress susceptibility through IGF-1-C/EBPβ-DRP1.
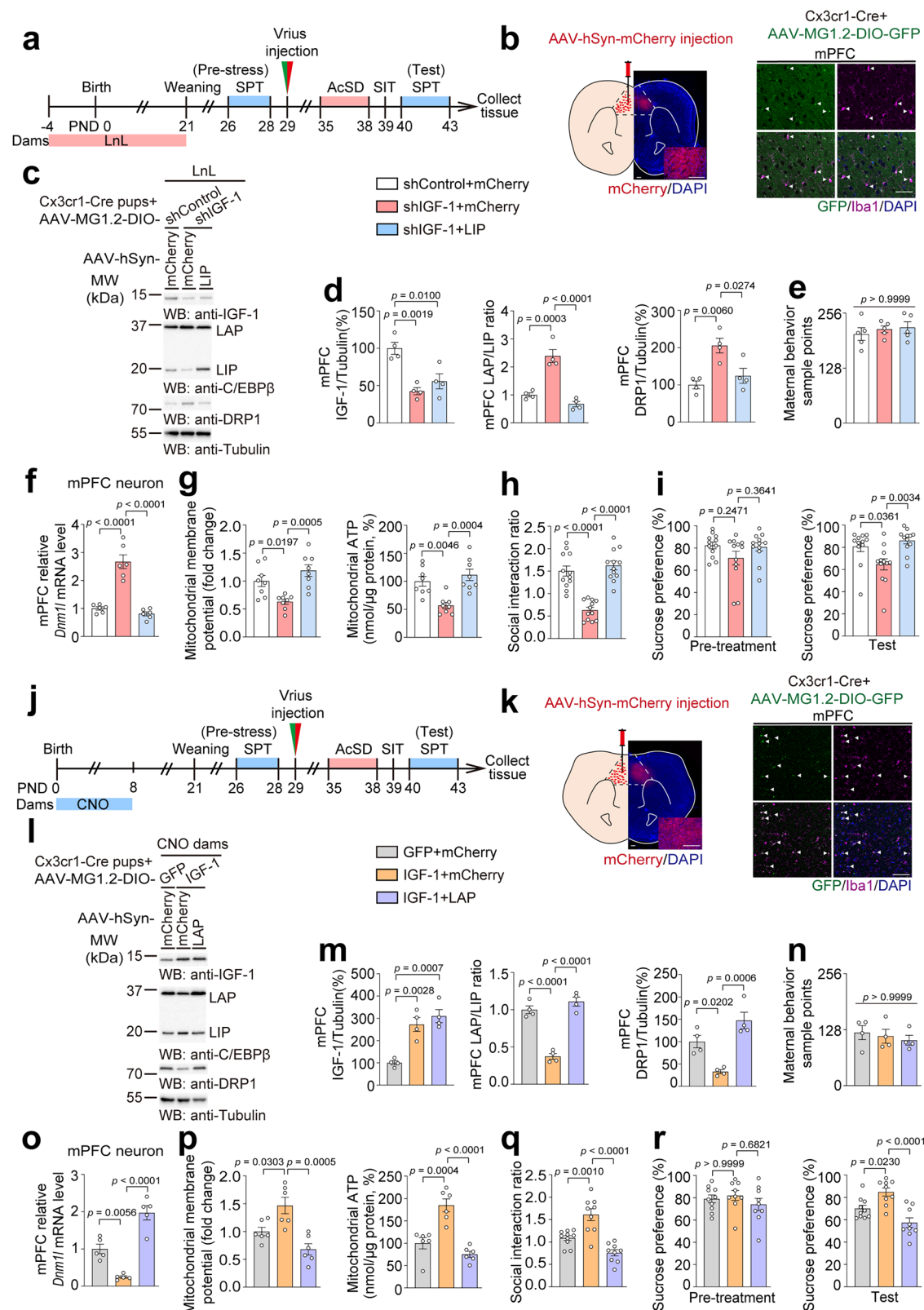
Discussion

Our study provides evidence that maternal behavior-mediated IGF-1-C/EBPβ-DRP1 signaling is important for the development of adolescent depression by modulating mitochondrial dysfunction (Fig. 9). Neuronal C/EBPβ activity in the mPFC of adolescent mice is markedly enhanced in response to AcSD, and this activated C/EBPβ transcription upregulates DRP1 expression, induces mitochondrial dysfunction and confers stress susceptibility. Importantly, this study demonstrates that maternal care for pups triggers elevated levels of microglia-derived IGF-1, which suppresses the neuronal C/EBPβ-DRP1 axis by modulating the LAP/LIP ratio, protecting the offspring from the "second hit" in the adolescence.

Firstly, utilizing a mouse model of accelerated social defeat-induced depression, we observed a significant association between stress susceptibility and mitochondrial dysfunction in the mPFC of adolescent mice. This association was effectively disrupted by a well-established DRP1 inhibitor, Mdivi1. We conducted further research into the protein expression and mRNA levels of DRP1 in adolescent mice subjected to the AcSD paradigm. Furthermore, immunostaining analysis revealed that social defeat-induced DRP1 expression was predominantly located in neurons of mPFC, rather than microglia or astrocytes. Next, we validated several transcription factors screened through ChIP-Atlas data in the susceptible mice, and found that C/EBPβ might be the transcription factor for *Dnm1l*. The results of luciferase assays, EMSA and ChIP experiments confirmed C/EBPβ as a transcriptional activator for *Dnm1l*. Notably, activated C/EBPβ was also localized in mPFC neurons, suggesting that the neuronal C/EBPβ-DRP1 axis is crucial for the development of adolescent depression. Moreover, specific overexpression or suppression of neuronal C/EBPβ-DRP1 in the mPFC effectively conferred or rescued stress susceptibility. MS, a classic early stress model, is closely related to adolescent depression. Our findings indicate that the C/EBPβ-DRP1 axis was inhibited in brief MS, but activated in prolonged MS, whereas IGF-1 levels in the mPFC

showed the opposite tendency. Further analysis confirmed that IGF-1 suppressed the neuronal C/EBPβ-DRP1 axis by activating the mTORC1 signaling, leading to a decreased LAP/LIP ratio. Additionally, the blockade or supplementation of IGF-1 regulated the C/EBPβ-DRP1 axis and AcSD-induced stress susceptibility in adolescent mice exposed to brief or prolonged MS. To better understand the association between different MS durations and stress susceptibility, we quantified maternal behavior in MS and control conditions, and found that brief MS increased maternal behavior while prolonged MS decreased it. This resulted in corresponding changes in IGF-1 levels in the mPFC of adolescent mice. Furthermore, we utilized LnL treatment or repeated inactivation of MPOA^{Esr1+} cells in dams to enhance or diminish maternal behavior. The results indicated the levels of maternal behavior in the early period impacted the neuronal C/EBPβ-DRP1 axis to prevent depressive-like behavior via IGF-1-mediated LAP/LIP ratio in the mPFC of adolescent mice. Since IGF-1 is a growth factor synthesized intracellularly and released outside the cell, we further measured and analyzed the *Igf1* mRNA levels in the mPFC. Our results demonstrated that *Igf1* mRNA levels also varied with changes in maternal behavior and were mainly produced from microglia in the mPFC. This suggests an important microglial-to-neuronal crosstalk in maternal behavior-mediated stress susceptibility. Thus, we used Cx3cr1-Cre mice and AAVs to specifically manipulate microglia-derived IGF-1 levels and neuronal C/EBPβ activity. The results of mitochondrial function assays and behavioral tests corroborate the assertion that microglial-to-neuronal IGF-1-C/EBPβ-DRP1 signaling plays a pivotal role in mediating stress susceptibility in the mPFC of adolescent mice.

Social defeat stress has been established as a reliable mouse model for studying adult depression, but a comparable experimental paradigm for adolescent depression has yet to be been widely recognized. Recently, Flores et al. reported an AcSD model that is effective in both adolescent male and female C57BL/6J mice[10,11,34]. In our study, screening of susceptible and resilient adolescent mice using the AcSD paradigm revealed mitochondrial dysfunction in the mPFCs of susceptible mice in both sexes. Mitochondrial dysfunction represents a significant mechanism in the pathogenesis of adult depression[30,31,60]. However, the association between adolescent depression and mitochondrial impairment has remained unclear. A growing body of evidence indicates that depressive behaviors in adolescents frequently co-occur with mitochondrial disorders[27,28]. Additionally, a transcriptome analysis demonstrates that adolescent stress response is

highly associated with mitochondria-related genes in the mPFC, and that mitochondrial respiratory capacity and hydrogen peroxide production rate are elevated in stressed adolescent mouse models[61]. Our findings support that AcSD paradigm in adolescent mice results in mitochondrial dysfunction through DRP1, including impaired MMP and decreased ATP levels.

Our results showed that social stress significantly increased mRNA and protein expressions of DRP1 in the mPFC of susceptible adolescent mice. However, in adult mice, social stress mainly upregulates phosphorylated DRP1 protein level, suggesting there may be different molecular mechanisms underlying susceptibility to stress in adolescent and adult mice[30]. The difference in mechanisms may be related to

Fig. 8 | Microglial-derived IGF-1 inhibits neuronal C/EBPβ-DRP1 axis to prevent stress susceptibility in adolescent mice. a Schematic representation of the experimental procedure of virus injection, and AcSD paradigm and behavioral tests for Cx3cr1-Cre mice with LnL dams. **b** The location of the cannula tips and fluorescence microscopy image of representative field showed mCherry expression in the mPFC injected with AAV-hSyn-mCherry; Fluorescence microscopy image of representative field showed GFP expression and Iba1 (Purple) in the mPFC injected with AAV-MG1.2-DIO-GFP in Cx3cr1-Cre mice. Scale bar: 100 μm (left), 50 μm (right). $n = 3$ mice for each group. **c, d** Representative immunoblots and quantification of LAP/LIP ratio, and IGF-1 and DRP1 expressions in Cx3cr1-Cre mice exposed to AcSD paradigm and virus injection of AAV-MG1.2-DIO-shControl or -shIGF-1 and AAV-hSyn-mCherry or -LIP, with LnL dams. Data are representative of three independent experiments. Data are presented the mean ± SEM ($n = 4$ for each group; one-way ANOVA and Bonferroni's multiple comparison test). **e** Measurement of maternal behavior sample points in Cx3cr1-Cre mice with indicative treatments. Data are presented the mean ± SEM ($n = 5$ for each group; one-way ANOVA and Bonferroni's multiple comparison test). **f** Measurement of *Dnm1l* mRNA levels in the mPFC neurons of Cx3cr1-Cre mice with indicative treatments. Data are presented the mean ± SEM ($n = 6$ for each group; one-way ANOVA and Bonferroni's multiple comparison test). **g** Measurement of mitochondrial MMP and ATP levels in the mPFC of Cx3cr1-Cre mice with indicative treatments. Data are presented the mean ± SEM ($n = 8$ for each group; one-way ANOVA and Bonferroni's multiple comparison test). **h, i** Behavioral tests of Cx3cr1-Cre mice exposed to AcSD paradigm and virus injection of AAV-MG1.2-DIO-shControl or -shIGF-1 and AAV-hSyn-mCherry or -LIP, with LnL dams. Measurement of social interaction ratio (**h**), and the percentage of sucrose preference (**i**) in Cx3cr1-Cre mice with indicative treatments. Data in (**h, i**) are presented as the mean ± SEM ($n = 12$ mice for each group; one-way ANOVA and Bonferroni's multiple comparison test). **j** Schematic representation of the experimental procedure of virus injection, and AcSD paradigm and behavioral tests for Cx3cr1-Cre mice with CNO-treated dams. **k** The location of the cannula tips and fluorescence microscopy image of representative field showed mCherry expression in the mPFC injected with AAV-hSyn-mCherry; Fluorescence microscopy image of representative field showed GFP expression and Iba1 (Purple) in the mPFC injected with AAV-MG1.2-DIO-GFP in Cx3cr1-Cre mice. Scale bar: 100 μm (left), 50 μm (right). $n = 3$ mice for each group. **l, m** Representative immunoblots and quantification of LAP/LIP ratio, and IGF-1 and DRP1 expressions in Cx3cr1-Cre mice exposed to AcSD paradigm and virus injection of AAV-MG1.2-DIO-GFP or -IGF-1 and AAV-hSyn-mCherry or -LAP, with CNO-treated dams. Data are representative of three independent experiments. Data are presented the mean ± SEM ($n = 4$ for each group; one-way ANOVA and Bonferroni's multiple comparison test). **n** Measurement of maternal behavior sample points in Cx3cr1-Cre mice with indicative treatments. Data are presented the mean ± SEM ($n = 4$ mice for each group; one-way ANOVA and Bonferroni's multiple comparison test). **o** Measurement of *Dnm1l* mRNA levels in the mPFC neurons of Cx3cr1-Cre mice with indicative treatments. Data are presented the mean ± SEM ($n = 5$ for each group; one-way ANOVA and Bonferroni's multiple comparison test). **p** Measurement of mitochondrial MMP and ATP levels in the mPFC of Cx3cr1-Cre mice with indicative treatments. Data are presented the mean ± SEM ($n = 6$ for each group; one-way ANOVA and Bonferroni's multiple comparison test). **q, r** Behavioral tests of Cx3cr1-Cre mice exposed to AcSD paradigm and virus injection of AAV-MG1.2-DIO-GFP or -IGF-1 and AAV-hSyn-mCherry or -LAP, with CNO-treated dams. Measurement of social interaction ratio (**q**), and the percentage of sucrose preference (**r**) in Cx3cr1-Cre mice with indicative treatments. Data in (**q, r**) are presented as the mean ± SEM ($n = 10$ mice for GFP + mCherry group; $n = 9$ mice for IGF-1 + mCherry group; $n = 9$ mice for IGF-1 + LAP group; one-way ANOVA and Bonferroni's multiple comparison test). See also Supplementary Fig. 19. Source data are provided as a Source Data file.

brain development. As shown in Supplementary Fig. 6h, the mPFC *Dnm1l* mRNA levels increased with age in wild-type non-stressed mice before adulthood (PND 0–60), suggesting that transcriptional regulation of *Dnm1l* plays a unique role in adolescence.

C/EBPβ is a transcriptional activator of *Dnm1l*, which affects mitochondrial activity. It is composed of a single exon, which produces a transcript that is translated into three protein isoforms: LAP*, LAP and LIP[62]. LAP* and LAP both possess transactivation domains and a DNA-binding domain whereas the LIP isoform lacks the N-terminal transactivation domains but retains the DNA-binding domain, thereby functioning as a competitive inhibitor for LAP* and LAP[63]. Notably, the LAP/LIP ratio indicates the C/EBPβ activity, with a high LAP/LIP ratio corresponding to high C/EBPβ activity. The expression ratio of C/EBPβ isoforms is regulated by the mTORC1-mediated translation initiation pathway. This pathway is activated by mTORC1 signaling, which in turn upregulates the translation of the LIP isoform[39]. The present study revealed that C/EBPβ activity varied with different MS durations. Specifically, LAP/LIP ratio decreasing in brief MS but increasing in prolonged MS. Furthermore, the neuronal C/EBPβ-DRP1 axis was inhibited by 10 min × 2 MS but activated by 180 min MS. Previous research has shown that brief MS prevents, while prolonged MS promotes, stress susceptibility in adolescent mice[64], which aligns with our findings on neuronal C/EBPβ activity. The contrary outcomes of MS may be due to increased maternal behavior in brief MS as an over compensatory response, though the detailed mechanism remains unclear. Our findings explain the conflicting effects of MS on adolescent depression and highlight the importance of maternal behavior during the early period of development. Owing to direct manipulation of transcription factor would produce unexpected side-effects, improving maternal behaviors may be a better prevention strategy.

Maternal behavior during the early period is critical for the neurodevelopment of offspring[65,66]. The quality and quantity of maternal care affects epigenetic changes in pups, such as DNA methylation and histone modifications[67]. Previous research has shown that maternal care alters methylation at the YY1 binding site in the promoter of long interspersed nuclear element-1 (LINE-1), inducing somatic mutation in the genome of pups[23]. Besides, maternal care affects cytosine methylation of the glucocorticoid receptor (GR) promoter, and modulates hypothalamic-pituitary-adrenal (HPA) responses to stress in offspring[21,68]. In the present study, in order to investigate innate maternal behavior, we observed spontaneous maternal behavior, including nursing postures, licking/grooming and nest building during PND 1–8, rather than passive maternal behavior such as retrieving pups from outside the nest. Moreover, to exclude the impact of breast milking, bodyweight of pups was measured and displayed no significant difference among maternal behavior inventions (Supplementary Figs. 11d, 14d). According to our experimental findings, we clarify that the effect of maternal behavior on adolescents experiencing stress is achieved by inhibiting the neuronal C/EBPβ-DRP1 axis, which is accomplished by increasing the level of IGF-1 released in microglia.

IGF-1 is a crucial hormone in the growth and development of the body during the postnatal and adolescent stages[69]. It can be synthesized in neurons and glial cells, while predominantly in the microglia during PND 4–7 mice[55]. Our current study reveals that microglia-released IGF-1, mediated by maternal behavior, prevents stress susceptibility in adolescent mice, highlighting the crucial role of IGF-1 in early development. Similarly, a recent study demonstrated impaired IGF-1 signaling in offspring that received reduced maternal behavior[70]. However, our study did not thoroughly investigate the detailed mechanism by which maternal behavior elevates microglia-derived IGF-1 levels. Some researchers revealed *E. coli* O16:H48 colonization in the dams impaired maternal behavior, resulting in inhibited IGF-1 signaling in the pups[70]. Additionally, methylation of CGs in the *Igf1* P2 promoter has been associated with the growth and development of offspring, indicating that maternal behavior may through DNA methylation to influence *Igf1* expression in the pups[21,71,72]. It can be postulated that intestinal microbiota control or epigenetic programming might be the possible mechanisms for elevated IGF-1 levels from microglia in pups with high maternal care.

In our experiments, IGF-1 released by microglia bound to its receptor on the neuronal surface and activated mTORC1 signaling, thereby reducing C/EBPβ activity, demonstrating an inhibitory effect
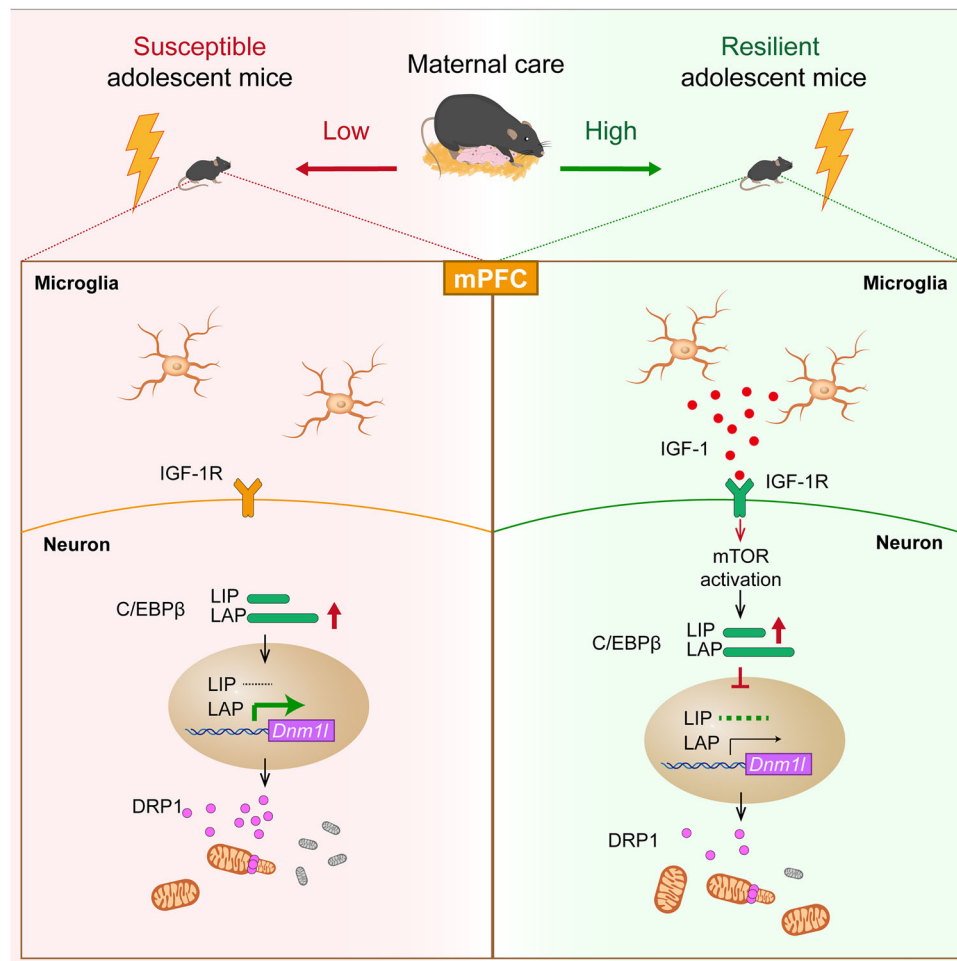
Fig. 9 | Maternal behavior in the early period can mediate later-life stress resilience by a microglial-to-neuronal IGF-1-C/EBPβ-DRP1 signaling in the mPFC of adolescent mice. In the mPFC of adolescent mice with low maternal care, social stress activates transcription factor C/EBPβ in mPFC neurons, upregulating *Dnm1l* expression and promoting mitochondrial dysfunction, which confers to stress susceptible in adolescent mice. However, high maternal care stimulates microglia to relieve IGF-1, which inhibit neuronal C/EBPβ activity through mTOR-induced C/EBPβ-LIP translation via binding to IGF-1R on the neurons in the mPFC of offspring, which protects stress resilience in adolescence. Source data are provided as a Source Data file.

of IGF-1 on C/EBPβ. Previous studies have also shown that IGF-1 signaling is the upstream of the PI3K/Akt/mTOR pathway through insulin receptor substrates[47]. In addition, activated mTORC1 reduces the LAP/LIP ratio by regulating translation initiation[39]. Interestingly, it has been shown that IGF-1 is also transcriptionally activated by the C/EBP family, and that C/EBPδ binds as a dimer to the HS3D site on the IGF-1 promoter and enhances transcription of the IGF-1 gene in osteoblasts[73]. Importantly, C/EBPβ is shown to be a positive transcription factor for IGF-1 in adult sensory neurons, ameliorating diabetes-induced dysfunction[74]. Therefore, there may be a bidirectional relation between IGF-1 and C/EBPβ in different conditions, which needs to be explored in more studies.

Owing to unstable hormone levels in female animals, male mice are primarily used in our experiments, which might ignore some sex-specific mechanisms. The discrepancy in the number of mice between the two species represents a major limitation of our study. Further studies on female adolescent mice are needed to investigate our findings regarding stress susceptibility. Besides, in current study, we pay more attention to maternal care by isolating pregnant mice from male mice, however in human real life both maternal and paternal care are indispensable to development of offspring. Paternal care may similarly display a crucial impact on social behaviors and stress response in the next generation[75]. Moreover, although our study focused on adolescent stress susceptibility, we showed that maternal

care-induced alterations in IGF-1 persisted until PND 60 in mice with a nonsignificant increase (Supplementary Fig. 17h, i). We did not delve into the intrinsic mechanism of how maternal behavior induces IGF-1 release from microglia, which needs to be explored in further studies.

Overall, our work clarifies that the microglial-to-neuronal IGF-1-C/EBPβ-DRP1 axis promotes the development of stress susceptibility in the mPFC of adolescent mice via mitochondrial dysfunction. Importantly, our results support that Mdivi1, a DRP1 inhibitor, can restore mitochondrial dysfunction and exert an anti-depressive effect in adolescent mice. This provides insights into the clinical management of adolescent depression. Moreover, our findings highlight that maternal behavior in the early period is protective for the offspring against depressive-like behavior in response to stress during adolescence, providing evidence for early intervention in adolescent depression.

Methods
Ethics approval statement
The Laboratory Animal Welfare Ethical Committee of Renmin Hospital of Wuhan University approved all animal experimental protocols (WDRM 20240503C). Animal care and handling were performed according to the NIH animal care guidelines and Wuhan University guidelines. All procedures involving animals were proved by the Institutional Animal Care and Use Committee of Renmin Hospital of Wuhan University.

Antibodies, virus, and chemicals

A detailed list of antibodies applied in the study, is provided in Supplementary Table 1 in Supplementary Data 1.

A detailed list of viruses applied in the study, is provided in Supplementary Table 2 in Supplementary Data 1.

A detailed list of chemicals applied in the study, is provided in Supplementary Table 3 in Supplementary Data 1.

Animals

The C/EBPβ heterozygous knockout (C/EBPβ+/-) mice and C57BL/6J mice (C/EBPβ+/+) were obtained from Jackson Laboratory (stock #006873 and #000664, respectively). Since the homozygous mutation of *Cebpb* is lethal on pure-strain backgrounds, the C/EBPβ knockout mice are maintained as heterozygotes on a C57BL/6 strain background. The Esr-2A-Cre mice (JAX strain #017911) was a gift from Dr. Xiaohong Xu. The Cx3cr1-iCre mice (Catalog C001391) were purchased from Cyagen.

Thy1-human C/EBPβ-LAP transgenic (Tg) mouse of C57BL/6J background were generously provided by Dr. Keqiang Ye. The generation of these LAP-Tg mice has been previously described[32]. Briefly, mouse genomic fragments were amplified from a bacterial artificial chromosome clone using high-fidelity Taq polymerase and assembled into a targeting vector. After verification via Southern blotting, correctly targeted clones were selected for blastocyst microinjection. Founders confirmed for germline transmission through crossbreeding with wild-type (WT) mice, and the F1 heterozygous mutant mice were identified as the final progeny. We conducted PCR to validate the genotypes of transgenic mice. Primer mixes #1 was used to distinguish between Non-Tg and LAP-Tg mice, with the forward primer sequence as TGAAGCATTCCCTAATGAGCCAC and the reverse primer sequence as CTCGCCTCCTCCGGCCACTGCTAG. Primer mixes #2 allowed for differentiation between Non-Tg, Tg, and Tg/Tg mice, with the forward primer sequences being AGAGTTGGTTGGTCCTCTCCT and the reverse primer sequence being GCCATTTAAGCCATGGGAAGTTAG.

Mice were distributed randomly among the groups using random number tables. Sample sizes were calculated using the Power and Precision software developed by Biostat. Mice were housed collectively in a 12-h light/12-h dark cycle at a constant temperature of 22 °C under specified pathogen-free (SPF) conditions. Both food and water were available ad libitum. Following behavioral assessments, mice were selected randomly from each group for subsequent analyses. All behavioral assessments were conducted without prior knowledge of the animals' treatment history. The Laboratory Animal Welfare Ethical Committee of Renmin Hospital of Wuhan University approved all animal experimental protocols (WDRM 20240503C). Animal care and handling were performed according to the NIH animal care guidelines and Wuhan University guidelines. All procedures involving animals were proved by the Institutional Animal Care and Use Committee of Renmin Hospital of Wuhan University.

Cell lines

HEK293 cells (CRL-1573) were obtained from the American Type Culture Collection (ATCC) and cultured in Dulbecco's Modified Eagle Medium (DMEM, Thermo Fisher, 11965092) supplemented with 10% fetal bovine serum (FBS, Thermo Fisher, 12483020) and 0.1% penicillin/streptomycin (Thermo Fisher, 15140122). The cells were incubated at 37 °C in a humidified atmosphere containing 5% CO_2 and 95% O_2, using a HERAcell Vios 160i incubator (Thermo Fisher).

Study design

At first, we utilized accelerated social defeat (AcSD) paradigm to induce depression in adolescent C57BL/6J WT mice. Through social interaction test (SIT), the mice exposed to AcSD were classified as susceptible and resilient groups. Mice without AcSD were considered as control group. The data in Fig. 1 and Supplementary Fig. 1 represent findings from AcSD-exposed mice and control mice. Mice of equal number were randomly taken from this pool of mice for further analysis in Figs. 1–4 and Supplementary Figs. 1, 2. The figures and figure legends showed the sample sizes. We found a significant association between stress susceptibility and mitochondrial dysfunction in the mPFC of adolescent mice, which was effectively disrupted by a DRP1 inhibitor, Mdivi1. To better understand this association, we quantified the protein and mRNA levels of DRP1 and clarified its location in cell type by immunostaining. Further knockdown and overexpression of DRP1 confirmed the relationship of DRP1-mediated mitochondrial dysfunction and stress susceptibility. To further investigate the transcription of *Dnm1l*, combining of ChIP-Atlas data and validation in susceptible mice, we found that C/EBPβ might be the transcription factor for *Dnm1l*. Luciferase assays, EMSA, ChIP experiments and primary mouse neurons confirmed C/EBPβ as a transcriptional activator for *Dnm1l*. Further overexpression or suppression of DRP1 in WT mice, C/EBPβ+/- mice and LAP Tg mice confirmed the molecular relationship between C/EBPβ and *Dnm1l*. To investigate the role of C/EBPβ-DRP1 axis in maternal separation, we conducted maternal separation on different durations and found that C/EBPβ-DRP1 axis was inhibited in brief MS while activated in prolonged MS, which was opposite with IGF-1 levels in the mPFC. Further experiments confirmed that IGF-1 suppressed the neuronal C/EBPβ-DRP1 axis by binding to IGF-1R and activating the mTORC1 signaling, leading to a decreased LAP/LIP ratio. Additionally, blocking or supplementing IGF-1 influenced the neuronal C/EBPβ-DRP1 axis and consequently stress susceptibility in adolescent mice experiencing brief or prolonged MS. To deeply exploration of C/EBPβ-DRP1 axis in maternal separation, we measured maternal behavior in MS on different durations and found that maternal behavior increased in brief MS but decreased in prolonged MS, which was consistent with changes in IGF-1 levels in the mPFC. Additionally, addition or reduction of maternal behavior in the early period further confirmed the IGF-1-C/EBPβ-DRP1 signaling in mediating depressive-like behaviors in adolescent mice. To further explore the source of IGF-1 levels, we measured and analyzed the *Igf1* mRNA levels in the mPFC, and confirmed that microglia was primary source of maternal behavior-induced IGF-1 through microglia depletion. Finally, we used Cx3cr1-Cre mice and AAV-hSyn virus to specifically manipulate microglia-derived IGF-1 levels and neuronal C/EBPβ-DRP1 axis, validating the IGF-1-C/EBPβ-DRP1 signaling in conferring depressive-like behavior in adolescent mice.

Accelerated Social Defeat (AcSD) paradigm

Attack definitions. To follow a standardized AcSD paradigm[10,11,34], we used the definitions of attack during AcSD paradigm as follows:

(1) One attack is described as when CD-1 mouse bites the C57BL/6J mouse, and the C57BL/6J mouse moves away as a defense to the bite.

(2) A bite is defined as when CD-1 mouse puts its teeth on any body part of the C57BL/6J mouse.

(3) The definition of moving away is when the C57BL/6J mouse moves both of its hind paws from the position they are in before CD-1 mouse engages it.

(4) There must be at least a 2-s pause between successive attacks. Multiple bites without a 2-s pause would be considered as a single attack.

(5) The operator would cautiously separate the animals if CD-1 mouse bites more than once in 2 s without a pause described in (4). These bites would be considered as a single attack.

(6) Gently separate the animals if CD1 mouse bites and refuses to release its hold.

(7) Gently separate the animals using a ruler if the C57BL/6J mouse become stuck in a corner or is pinned down by CD-1 mouse and unable to escape after being bitten.

Adolescent AcSD, priming and screening for aggression. CD-1 mice were trained for aggression in two periods prior to AcSD sessions. In the first period of 3 days, an adult male C57BL/6 mouse (PND 65) was placed in the home cage of a CD-1 mouse and left there for 3 min, or until it was attacked ten times. The second period began on the 4th day, which involved priming twice a day at 9:00 and 14:00. During this period, an adolescent C57BL/6J mouse (PND 34–35) was placed to the CD-1 mouse's home cage for 5 min after an adult C57BL/6 mouse had just been there for thirty seconds. The second period continued for 3–4 days, or when a subset of CD-1 mice started acting aggressively against the teenage C57BL/6J mice on a regular basis. The latency and attack number of CD-1 mice were recorded in the second period. The CD-1 mice, which attacked the C57BL/6J mice for at least 10 times or 2 days in a row, were chosen to be aggressors in the AcSD. The C57BL/6J mice used in priming procedure were not involved in other experiments.

Adolescent AcSD, social defeat sessions. The AcSD apparatus consists of a transparent rat cage with two mouse housing compartments divided by a perforated, transparent center divider that permits sensory but not physical contact between mice. To improve the CD-1 mice's territorial behavior, each chosen CD-1 mice that have been previously screened for aggressive behavior was kept in one of the compartments for at least 48 h prior to the start of AcSD. The other compartment was still vacant. We performed the priming phase 2 again the day before the experiment to make sure CD-1 mice remaining aggressive toward adolescent C57BL/6J mice. The AcSD protocol was held on 9:00 and 14:00 sessions every day for a total of 4 days. To prime the CD-1 mice for aggressive behavior, an adult C57BL/6 mouse was placed into the CD-1 compartment for 30 s at each session. Then, the adult C57BL/6 mouse was taken out, and an adolescent C57BL/6J mouse (PND 35) was added as an intruder. The adolescent C57BL/6J was left with CD-1 mouse until 10 min has passed or ten attacks have taken place, whichever came first. The C57BL/6J adolescent mouse was kept overnight on the empty compartment after the session to induce psychological stress. Adolescent C57BL/6J mice were given a daily exposure to a new aggressor. Adolescent C57BL/6J control mice were kept in daily, identical, two-compartment cages with a conspecific every day. For the remaining parts of the behavioral trials, each mouse was placed in its own cage following the last AcSD session on day 4.

Subthreshold Social Defeat (SSD) paradigm
As for the priming and screening parts, SSD shared the same steps with AcSD. In social defeat session, the SSD followed the procedure in AcSD, but just lasted 1 day.

Social interaction test (SIT)
The SIT was performed in a rectangular chamber (45×45 cm^2) with two corner zones (10×10 cm^2) and an interaction zone (14×16 cm^2), and the interaction behavior of mice was tracked by VisuTrack software. There were two sessions in the social interaction test. Firstly, the test mouse was placed into the chamber and allowed to explore freely for 2.5 min. Next, a novel CD-1 mouse was placed into the cage within the interaction zone, and the test mouse was introduced into the chamber for another 2.5 min. The time the test mouse spent in the interaction zone and corner zones with or without the target of CD-1 mouse was recorded. Social interaction ratio was calculated based on the time spent in the interaction zone with target by dividing that without target. The mouse with social interaction ratio <1.0 was considered susceptible and that with social interaction ratio ≥1.0 was considered resilient. The observers were blinded to the treatment the mice received when evaluating the data.

Sucrose preference test (SPT)
The SPT was widely used to examine anhedonia, which was a key feature of depression and defined as a sucrose preference level below

65%[76]. Before the AcSD paradigm was started, adolescent mice were accustomed to having two drinking tubes (50 mL Falcon® with siliconized rubber stops and stainless-steel sipper tubes) in their home cages: one containing tap water and the other containing 1% sucrose solution. Previous research has demonstrated that 1% sucrose solution produced a strong sucrose preference (~80% over tap water) in adolescent C57BL/6J male mice[77]. The acclimatization was repeated after the AcSD paradigm. After the acclimatization, the drinking sessions lasted from 17:00 to 21:00, and the consumption of each mouse was measured by weighing the bottles before and after the sessions. Tap water was freely available to mice in between drinking sessions. To determine sucrose preference percentage, the amount of sucrose solution consumed was divided by the total intake of both the sucrose solution and regular water during the 4-h test. The observers were unaware of the treatment given to the mice when evaluating the results.

Open-field test (OFT)
The OFT procedure has been described in our previous study with slight modifications[32]. In brief, mice were allowed to explore a white plastic chamber ($40 \times 40 \times 40$ cm^3) for 10 min. Behaviors were recorded using a video camera and subsequently analyzed with the VisuTrack software.

Elevated plus maze test (EPM)
The EPM method has been described before[32]. Mice were habituated for 5 min on a plus-shaped platform consisting of two open arms ($30 \times 5 \times 0.5$ cm^3), two closed arms ($30 \times 5 \times 15$ cm^3), and a central connecting zone (5×5 cm^2) 1 day before the test. On the test day, mice were placed on the center platform of the maze and allowed to explore the open arms for 5 min. Their movements were recorded using a video camera positioned above the central zone and subsequently analyzed with VisuTrack software.

Chronic unpredictable stress (CUS) paradigm
This method has been described in our previous study[32]. Every mouse used in the CUS paradigm has its own housing cage and was allowed to adapt to a 1% sucrose solution for 2 days. After that, for a duration of 5 weeks, mice were randomly assigned to 2–3 stressors each day. These stressors included a 24 h period without food or water, a 1 h period of cold exposure at 4 °C, a 12 h period with wet bedding, a 1 h period of restraint, a 12 h period without bedding, a reversal of the light-dark cycle, a 12 h period under strobe lighting, a 10-min swim stress in 18 °C water, and foot shocks delivered 10–20 times with intervals ranging between 5 and 30 s at an intensity of 0.5 mA.

Microarray data
Gene Expression Omnibus (GEO) database is a public database consisting of high-throughput gene expression data (https://www.ncbi.nlm.nih.gov/geo). We screened brain samples from patients with major depression disorder in the GEO database and selected dataset GSE54568. This dataset includes 30 total samples in 15 pairs of postmortem tissue from the dorsolateral prefrontal cortex. From the GEO (GPL570 Affymetrix Human Genome U133 Plus 2.0 Array), we downloaded the gene expression datasets and the probe information for GSE54568 to analyze the expression level of *Dnm1l* and *Cebpb* gene.

Transcription factor prediction of the *Dnm1l* gene
Transcription factor prediction was made through the Signaling Pathways Project (SPP) link in the website (http://www.signalingpathways.org/index.jsf)[78]. The SPP project provided possible transcription factors along with binding scores for *Dnm1l* gene. We searched for the transcription factors in commonly used cell lines HeLa S3, and the relative expressions of transcription factor genes were detected using qPCR.

ChIP-seq database screening and GSM select

To understand the conservativeness of C/EBPβ binding with *Dnm1l*, we searched for ChIP-seq data about C/EBPβ binding with *Dnm1l* in Cistrome.db website (http://dbtoolkit.cistrome.org)[79]. We got 4 representative Sample (HeLa cells GSM935553, HepG2 cells GSM935622, HCT116 cells GSM1010852, MSCs cells GSM1684642) showing that C/EBPβ bound to the promoter region conservatively in different cell lines and tissue.

Prediction of C/EBPβ binding motif

The DNA sequence of the mice *Dnm1l* was obtained from the UCSC genome browser (https://genome.ucsc.edu.). The binding motifs of C/EBPβ on mice *Dnm1l* promoter were analyzed by JASPER online tools (https://jaspar.elixir.no)[80]. The Relative profile score thresholds were set at >85%.

Luciferase assay

HEK293 cells were co-transfected with different truncates of *Dnm1l* promoter luciferase reporters and GST-vector or GST-C/EBPβ plasmids, and cultured for 36 h. According to the manufacturer's suggested protocol (Promega), cells were harvested by a passive lysis buffer and then analyzed by a Dual-Luciferase Reporter Assay System. Relative luciferase activities of different truncates of *Dnm1l* promoters were normalized to Renilla luciferase activities to control. The experiments were repeated three times.

EMSA (Electrophoretic Mobility Shift Assay; DNA: protein)

The LightShift Chemiluminescent EMSA Kit (Life Technologies) was used to conduct the EMSA assay. Nuclear proteins were extracted using the Nuclear and Cytoplasmic Protein Extraction Kit (Beyotime Biotech, P0028). Utilizing Pierce™ BCA Protein Assay Kits (Thermo Fisher, 23227), protein concentrations were determined. Based on the prediction results, double-stranded oligonucleotide probes were designed for the Site 4 of the *Dnm1l* (−1369 to −1060) promoter and labeled with biotin. Unlabeled probes (cold probes) worked as competitors. Mutant probes labeled with biotin served to confirm the binding specificity. The binding of C/EBPβ was verified using the C/EBPβ antibody (supershift), but not to any other transcription factors. The primer sequence for the binding site 4 as: AATGCAGTGGCGCAATCTCG, and the mutant primer sequence as: AATGCAGTGTATCAATCTCG.

Chromatin immunoprecipitation (ChIP)

HEK293 cells were fixed with 1% formaldehyde for 10 min and the cross-linking was quenched with 2 M glycine for 5 min. After isolation of nuclei, chromatin was sonicated using a Covaris S220 sonicator to obtain the desired DNA fragment size (-500 bp). The sonicated chromatin was pre-cleaned by twice-centrifugation at maximum speed at 4 °C. Then, 5 μL of anti-C/EBPβ or anti-IgG were used to precipitate the chromatin fragments containing DNA-protein cross-linking ChIP samples, which were collected with 50 μL Dynabeads Protein A (Invitrogen, 10001D). The PCR assay assessed the enrichment of specific DNA sequences, and detected each input sample. The positive control was demonstrated with anti-Histone H3 antibody coupling with GAPDH primers. Following 35 PCR cycles (denature for 30 s at 95 °C, anneal for 30 s at 58 °C, and extend for 30 s at 58 °C), the PCR amplicon was separated using a 2% agarose gel.

Maternal separation (MS)

The day of birth is postnatal day 0 (PND 0). According to Andersen and Weiss's instructions, [81–83]MS was carried out on PND 1. During the separation, dams were removed from the maternity cage and the pups were weighed and replaced in the other cage for the rest of the experiment. The cage contained 3-cm bedding and was placed on a heating pad set at 37 °C. At the end of the separation period, the dams and pups were returned to their original cages. All litters were weaned at PND 21, and housed in groups of 5–6 mice of the same sex for the following behavioral test.

In our study, the pups were assigned randomly into one of five conditions: the short maternal separation groups (MS for 20 min × 1 or 10 min × 2): pups were exposed to 20 min of MS during PND 1–21; the long maternal separation groups (MS for 180 min × 1 or 90 min × 2): pups were separated from their dams as a litter for 180 min during PND 1–21; and the control group (without MS): pups were only replaced the bedding of their cages until PND 10. The separation period started at 18:00 in MS for 20 min × 1 and 180 min × 1, while at 10:00 and 18:00 in MS for 10 min × 2 and 90 min × 2, respectively.

Maternal behavior sample points

Maternal-infant interaction was recorded in the animal room during PND 1–8. Assessments were made by calculating the number of maternal behavior sampling points. The rules for calculating the sampling points are as follows[49,84].

Maternal behavior was recorded twice a day in 8:00–9:00 and 16:00–17:00 in different maternity cages by a SONY video recorder. Daily monitoring consisted of 32 sample points in total, and each sampling point referred to the first 5 s of every 4-min period in each sampling time period. If the dam showed any of maternal behavior as following described, the cage got one sample point. If in 5 s period the dam showed more than single maternal behavior or more than once, we just calculated this 5-s period as one sample point.

The following maternal behaviors are observed:
(1) nursing postures (NP), that is, arched-back nursing (the dam is in an arched position over the nursing pups) and blanket nursing (the dam is lying flat on top of the pups);
(2) licking/grooming of the pups, body licking, and anal licking included;
(3) nest building, that is, the dam is pushing and retrieving the nesting materials around the pups.

Lactating and non-Lactating mother model

Previous studies have the similar paradigm[49,84]. A few days prior to the birth, female pregnancy mouse was isolated (control condition, L = Lactating) or housed with an age-matched unfamiliar virgin C57BL/6J female mouse (LnL condition, LnL = Lactating and non-Lactating). Three cohorts of female mice were used to generate all mice used in different experiments. Housing conditions and indoor temperature were constant with a 12 h:12 h light: dark cycle. A standardized amount of bedding and nesting material (soft paper) was provided for each cage. Around the day of birth, cages were checked twice a day for newborn pups, in which case PND 0 was set. Pups were counted on PND 1, leaving the unchanged number of pups in each cage. Dams with fewer than four pups during the whole process were not included in the experiments. The detailed lists for the exact number of litters included in the LnL model, are provided in Supplementary Table 4 in Supplementary Data 1. When more than 3 cages are used for maternal behavior sample points, we randomly select 3 cages of litters for subsequent experiments. Cage bedding was not cleaned until PND 10, and maternal behavior was assessed as previous statement during PND 1–8.

Stereotactic injection of viruses, antibody to IGF-1, or drugs

Mice were anesthetized with isoflurane (Sigma-Aldrich, PHR2874) and fixed to a specialized mouse frame (RWD Life Science).

For mPFC virus injection, we used a glass capillary with nanoinjector (World Precision Instruments, Nanoliter 2000) to inject reagents into mPFC (anteroposterior: +1.80 mm, transverse: ±0.30 mm and dorsoventral: −2.10 mm) in PND 29 mice at a 20 nL/min rate or specially mentioned.

For MPOA virus injection of Esr1-2A-Cre female mice, virus was stereotactically injected into the MPOA (anteroposterior: +0.02 mm,

transverse: ±0.325 mm, dorsoventral: −5.10 mm) bilaterally through a glass capillary using nanoinjector (World Precision Instruments, Nanoliter 2000) at 20 nL/min or specially mentioned. One week after the surgery, the female mice were paired with males until the female mice became visibly pregnant.

According to Shuai Liu's instruction[85], we performed cannulation infusion. For mPFC cannulation and drug infusion, guide cannulas were implanted bilaterally into the mPFC (anteroposterior: +1.80 mm, transverse: ± 0.30 mm, dorsoventral: − 1.80 mm) in PND 29 or 30 mice. For intracerebroventricular (i.c.v.) injection, guide cannulas were implanted in the following coordinates: right lateral ventricle (anteroposterior: +0.74 mm, transverse: +0.80 mm, dorsoventral: −2.10 mm) in PND 29 or 30 mice. The cannulas were secured to the skull using dental acrylic. The mice were housed individually and allowed to recover for at least 7 days after surgery. After a 7-days recovery, Mice were bilaterally infused with antibodies, mouse recombinant IGF-1 or drugs using an injector that protruded 0.3 mm beyond the tip of the guide cannula. Appropriate positive pressure was applied by a microsyringe pump to infuse the drug or antibody at a rate of 0.2 μL/min or specially mentioned. The injection rates and dose of drugs and antibodies are showed in "*Preparation and administration of test agents*".

Surgical procedures were approved by the Institutional Animal Care and Use Committee of Renmin Hospital of Wuhan University. A randomized block design was used to assign mice to age-matched treatment groups. A detailed list of coordinates of virus injection or cannulation used in the study, is provided in Supplementary Table 5 in Supplementary Data 1.

Preparation and administration of test agents

For systemic administration, fluoxetine hydrochloride was dissolved in distilled water at the concentration of 2 mg/mL, and intraperitoneally injected once for 6 days with the dose of 20 mg/kg.

CNO was dissolved in saline at the concentration of 2 mg/mL, and intraperitoneally injected to lactating dams with the dose of 1 mg/kg twice a day 10 min prior to maternal behavior recording, to silence cells expressing hM4Di-mCherry.

GW0742, a PPAR-δ agonist, was dissolved at the final concentration of 50 mM in a solution consisting of 98% ACSF, 1% Tween-80, and 1% dimethyl sulfoxide. The final concentration of GW0742 in in vivo experiments was 50 mM. The injection rate was 0.2 μL/min while the volume was 1 μL/side once a day.

Mdivi1 was dissolved at the final concentration of 100 μM in ACSF. The final concentration of GW0742 in in vivo experiments was 100 μM. The drug was injected into the mPFC at a rate of 0.5 μL/min while the volume was 1.5 μL/side once a day.

The IGF-1 nAb (R&D Systems, AF791) or control IgG (R&D Systems, AB-108-C) was diluted in PBS, and injected into the bilateral mPFC with 160 ng each side at a rate of 0.2 μL/min once a day.

IGF-1 was diluted in PBS, and injected into the bilateral mPFC with 50 ng each side at a rate of 0.2 μL/min once a day.

PLX3397, colony-stimulating factor 1 receptor (CSF1R) inhibitor, was dissolved at the final concentration of 100 μM in 10% DMSO and 90% sulfobutylether-β-cyclodextrin (SBE-β-CD). Mannosylated clodronate liposomes (MCLs) was applied to polarized microglia in vivo to assess specificity in promoting anti-inflammatory phenotype of microglia apoptosis. PLX3397 (100 μM in 2 μL) or MCLs (20 μL) was injected into the right lateral ventricle through the intracerebroventricular (i.c.v.) injection cannulas at a rate of 0.2 μL/min. The needle remained in place for 5 min after injection of the drugs, followed by slow removal.

Anti-IL-6 antibody was diluted in PBS, and at the concentration of 0.5 mg/mL, and intraperitoneally injected once in control and susceptible adolescent mice with the dose of 5 mg/kg.

The time point and duration of drug administration was detailed described in the schematic time line. A detailed list of the dose and injection rate of drug administration used in the study, is provided in Supplementary Table 6 in Supplementary Data 1.

Primary culture of mouse cortical neurons

Cerebral cortices from E16 to E18 C57BL/6J mice were carefully dissected, with meninges removed under a dissecting microscope. The whole process of dissection was carried out in cold DMEM (Thermo Fisher, 11965092). Tissues were finely minced to 1 mm³ using scissors and subsequently transferred to a new dish containing 4 mL of DMEM supplemented with 2 mg/mL papain (MedChem Express, HY-P1645). The tissue fragments were digested in an incubator at 37 °C in 5% CO_2 and 95% O_2 for 30 min, with gently swirling every 5 min. Following digestion, the papain-containing medium was aspirated and replaced with 4 mL of inoculation medium (DMEM + 5% FBS + 5% horse serum, Thermo Fisher, 16050122) to stop the digestion. The mixture was then gently pipetted -10 times and left on ice for 2 min before 2 mL of the supernatant suspension was transferred to a new tube. We then added another 2 mL inoculation medium to the tissue mixture and replicated the above process. After repeating the process twice, a total of 6 mL of supernatant was collected and centrifuged at $200 \times g$ for 10 min. The supernatant was discarded, and the resultant cell suspension was resuspended in 2 mL of the same inoculation medium. Cells were counted and seeded on 6-well plates pre-coated with poly-ethyleneimine (PEI; Sigma-Aldrich, P3143) at densities ranging from 4×10^5 to 7×10^5 cells per well. After 4 h of incubation, the inoculation medium was replaced with Neurobasal medium (Thermo Fisher, 21103049) supplemented with 0.5 mM glutamine (Thermo Fisher, 35050061), 1% penicillin/streptomycin, and 2% B-27 supplement (Thermo Fisher, 17504044). The medium was refreshed every 4 days by replacing half of the initial volume.

Magnetic bead sorting-based isolation of neurons and microglia

Neuron and microglia isolation from adolescent brains were conducted according to recent studies and the manufacturer's protocol from Miltenyi Biotec[86–88]. Adolescent mice anesthetized with isoflurane (Sigma-Aldrich, PHR2874) and perfused transcardially with Hanks' balanced salt solution (HBSS) buffer. mPFC tissues were quickly collected and cut into small pieces on the ice, then homogenized gently using a Dounce homogenizer. After filtered with 70 μm cell strainers, the tissue homogenates were centrifuged at $600 \times g$ for 6 min. Then, the debris removal solution was added to the cell pellets, in order to remove cell debris, then centrifuged at $3000 \times g$ for 10 min. Isolated cells were washed with 10× volumes of HBSS and centrifuged at $1000 \times g$ for 10 min. Neurons and microglia were further respectively sorted by Neuron isolated kit II (Miltenyi Biotec 130-115-389) and CD11b microbeads (Miltenyi Biotec 130-093-634) according to the manufacturer's guideline.

Cell transfection and treatment

We transfected HEK293 cells using Lipofectamine 2000 (Invitrogen, 11668019) according to the manufacturer's recommendations. For the treatment of primary neurons, IGF-1 or Vehicle was added into the culture medium for 72 h at a concentration of 20 nM.

Tissue lysis and western blotting

Brain tissues were washed with cold PBS and homogenized in RIPA buffer (Beyotime Biotech, P0013B) supplemented with phosphatase and protease inhibitors (MedChem Express, HY-K0010 and HY-K0021, respectively). The homogenates were sonicated four times for 5 s each and centrifuged at $17,000 \times g$ for 20 min at 4 °C. The supernatant was collected, and protein concentration was standardized to 5–10 mg/mL using Pierce™ BCA Protein Assay Kits (Thermo Fisher, 23227). Cytoplasmic and nuclear proteins were extracted using the Nuclear and Cytoplasmic Protein Extraction Kit (Beyotime Biotech, P0028). Protein samples were denatured in SDS loading buffer (Bio-Rad, 1610747) at

95 °C for 10 min, separated by 8–12% SDS-PAGE, and transferred to nitrocellulose membranes (Bio-Rad, 1620112). Membranes were blocked with 5% skim milk in TBS containing 0.1% Tween-20 (TBS-T) for 1 h at room temperature, then incubated with primary antibodies overnight at 4 °C. After 4–6 washes in TBS-T, the membranes were incubated with horseradish peroxidase (HRP)-conjugated secondary antibodies (anti-mouse, 1:5000, BL001A; anti-rabbit, 1:5000, BL003A, Biosharp Life Sciences, China) for 1 h at room temperature. Following five washes with TBS-T, the membranes were developed using enhanced chemiluminescence reagents and imaged with the ChemiDoc™ Touch Imaging System (Bio-Rad, 1708370). Band intensity was quantified using ImageJ software, and experiments were repeated and analyzed at least three times.

Enzyme-linked immunosorbent assay (ELISA)
Enzyme-linked immunosorbent assays were conducted according to the manufacturer's instructions (IL-6 mouse ELISA kit, Thermo Fisher, BMS603HS; TNF-α mouse ELISA kit, Thermo Fisher, BMS607-3; IGF-1 mouse ELISA kit, Thermo Fisher, EMIGF1; TransAM® C/EBP α/β, Active Motif, 44696). The protein concentrations were normalized by Pierce™ BCA Protein Assay Kits (Thermo Fisher, 23227). All samples were measured as doublets for technical replicates.

RNA isolation and quantitative real-time PCR (qRT-PCR)
Total RNA was isolated from tissue samples using the FastPure Cell/Tissue Total RNA Isolation Kit (Vazyme, RC112-01, China). RNA concentrations were determined with the Nanodrop apparatus (Thermo Scientific).

Synthesis of full-length first-strand cDNA was performed using 500 ng of total RNA with the HiScript III 1st Strand cDNA Synthesis Kit (Vazyme, R312-01, China). Quantitative real-time PCR (qRT-PCR) was carried out on 2 μL of cDNA using the Bio-rad Real-Time PCR System, with each sample run in triplicate in a 20-μL reaction volume. Primers for GAPDH and gene-specific sequences were obtained from TaqMan® (Thermo Fisher Scientific). Amplification settings were 95 °C for 30 s, followed by 40 cycles at 95 °C for 10 s and 60 °C for 30 s. The Taq Pro Universal SYBR qPCR Master Mix (Vazyme, Q712-02, China) was used. Gene expression was quantified using the ΔΔCt method, normalized to GAPDH mRNA levels, and expressed relative to controls.

Immunofluorescence staining
For the immunofluorescence, we used 20 μm brain sections. After three PBS washes, the brain sections were blocked for 30 min with 3% bovine serum albumin (BSA, w/v) and 0.3% Triton X-100 (v/v), and then incubated with primary antibodies at 4 °C overnight. On the 2nd day, the brain sections were incubated with a combination of labeled secondary antibodies for 2 h at room temperature, following three PBS washes. Finally, nuclei were stained for 5 min using DAPI (1:1000), and then the brain sections were rinsed three times with PBS. The images were captured by Leica Confocal Imaging System.

Fluorescent in situ hybridization (FISH) combination with immunostaining
For fluorescent in situ hybridization (FISH), ACD RNAscope® Kit (cat# 323100) was used according to the manufacturer's protocol. After balanced to room temperature and washed with PBS three times, fresh frozen brain slices (15 μm) were baked at 60 °C for 30 min, then fixed with ice-cold 4% paraformaldehyde at 4 °C for 15 min, followed dehydrated in anhydrous ethanol and dried at room temperature. The brain slices were incubated with RNAscope hydrogen peroxide at room temperature for 10 min. After washing, the brain slices were put into the target repair solution at 100 °C for 5 min for target repairment. Next, primary antibodies were added in the brain slices with a hydrophobic circle at 4 °C overnight. On the next day, the brain slices were again fixed with 4% paraformaldehyde at 4 °C for 15 min after washed

with PBST for three times. Following that the RNAscope protease plus was incubated with brain slices at 40 °C for 30 min, the brain slices were incubated in the hybridization oven at 40 °C for 2 h with probes (RNAscope™ 2.5 LS Probe-Mm-Dnm1l, ACD, Cat No. 434678; RNAscope™ 2.5 LS Probe-Mm-Igf1-C3, ACD, Cat No. 443908-C3). After hybridization, Amp1, Amp2, and Amp3 were successively incubated with the brain slices at 40 °C for 30 min. Then, HRP, fluorescent dye, and HRP blocker were added following closely at 40 °C for 15 min. Lastly, the corresponding fluorescent secondary antibodies were incubated with brain slices at room temperature for 30 min. Nuclei were stained for 5 min using DAPI (1:1000), and then the brain sections were rinsed three times with PBS. The images were captured by Leica Confocal Imaging System.

Transmission electron microscope
Mice were anesthetized and perfused with 2.5% glutaraldehyde, and the mPFC was isolated and post-fixed in 2.5% glutaraldehyde overnight at 4 °C. After washing with PBS, the mPFC was fixed in 1% OsO$_4$ in 0.1 M phosphate buffer (PB, pH 7.4) for 2 h at room temperature and dehydrated in a series of ethanol solutions (30%, 50%, 80%, and 100%) for 20 min each. The samples were then immersed in 100% acetone twice (15 min), and were infiltrated and embedded using EMBed 812 in acetone (1:1), followed by polymerization at 60 °C for 48 h. Sections were cut to 400 nm thickness using an ultramicrotome and placed onto 150-mesh copper grids coated with formvar film. The sections were stained with a 2% uranium acetate saturated alcohol solution for 8 min, rinsed three times in 70% ethanol, and then rinsed three times in ultrapure water. After staining with 2.6% lead citrate, avoiding CO$_2$ exposure, for 8 min, the sections were rinsed again with ultrapure water, dried, and observed using a HITACHI HT7800 transmission electron microscope at 80 kV.

Mitochondrial membrane potential assay
For the determination of mitochondrial membrane potential (MMP), the JC-1 assay kit (Beyotime) was used according to the manufacturer's protocol. First, mitochondria of mPFC and hippocampus were extracted quickly using the mitochondrial Extraction Kit (Beyotime), then added with JC-1 for 30 min at 37 °C in a 5% CO$_2$ incubator. After washed with PBS, fluorescence signals were measured at 490 nm excitation (ex)/530 nm emission (em) for JC-1 monomer and 525 nm excitation (ex)/590 nm emission (em) for the aggregates of JC-1. Carbonyl cyanide 3-chlorophenylhydrazone (CCCP) was added as a positive control by depolarization.

Quantification of ATP
The ENLITEN ATP Assay System Bioluminescence Detection Kit (Promega) was utilized to quantify the concentration of ATP. After cleaned with ice-cold PBS, the mPFC or the hippocampus tissues was homogenized in Krebs-Ringer bicarbonate HEPES buffer. The lysates were separated into 96-well plates and mixed with a 100 μL luciferin-luciferase reaction buffer. Utilizing a Biotek Synergy 2 SL Microplate Reader (BioTek), the luminescence was determined. The ATP levels were assessed by a standard curve and adjusted based on protein levels.

Statistical analysis
The sample size and outcome analysis for each group presented in the figure and figure legends. All data were analyzed by using GraphPad Prism 9.0 and presented as the mean ± standard error of the mean (SEM) from at least three independent experiments. The figure legends listed all the statistical procedures, including statistical tests, the number of samples. For the two groups, an unpaired *t*-test with Welch's correction was employed. For the three or more groups, one-way ANOVA followed by Bonferroni's multiple comparison test was used. The two-way ANOVA and Bonferroni's multiple comparison test was

employed to the groups with two independent factors. Values of $p < 0.05$ indicated statistical significance. The detailed lists for statistical values are provided in Supplementary Table 7 in Supplementary Data 1.

Reporting summary

Further information on research design is available in the Nature Portfolio Reporting Summary linked to this article.

Data availability

All data generated in this study are provided in the Supplementary Information/Source Data file. The expressions of *Dnm1l* and *Cebpb* mRNA in the brain samples from patients with major depression disorder were acquired from the GEO database under accession numbers GSE54568. The uncropped Western blots are also provided in the source data file. Source data are provided with this paper.

References

1. Gilmore, K. J. & Meersand, P. *Normal Child and Adolescent Development: A Psychodynamic Primer* (American Psychiatric Publishing, 2013).
2. Nansel, T. R. et al. Bullying behaviors among US youth: prevalence and association with psychosocial adjustment. *JAMA* **285**, 2094–2100 (2001).
3. Ttofi, M. M. Adolescent bullying linked to depression in early adulthood. *BMJ* **350**, h2694 (2015).
4. Altemus, M., Sarvaiya, N. & Neill Epperson, C. Sex differences in anxiety and depression clinical perspectives. *Front. Neuroendocrinol.* **35**, 320–330 (2014).
5. Forbes, E. E. et al. Healthy adolescents' neural response to reward: associations with puberty, positive affect, and depressive symptoms. *J. Am. Acad. Child Adolesc. Psychiatry* **49**, 162–172 (2010). e161-165.
6. Patton, G. C. & Viner, R. Pubertal transitions in health. *Lancet* **369**, 1130–1139 (2007).
7. Shorey, S., Ng, E. D. & Wong, C. H. J. Global prevalence of depression and elevated depressive symptoms among adolescents: a systematic review and meta-analysis. *Br. J. Clin. Psychol.* **61**, 287–305 (2022).
8. Collaborators, G. M. D. Global, regional, and national burden of 12 mental disorders in 204 countries and territories, 1990-2019: a systematic analysis for the Global Burden of Disease Study 2019. *Lancet Psychiatry* **9**, 137–150 (2022).
9. Nestler, E. J. & Russo, S. J. Neurobiological basis of stress resilience. *Neuron* **112**, 1911–1929 (2024).
10. Vassilev, P. et al. Unique effects of social defeat stress in adolescent male mice on the Netrin-1/DCC pathway, prefrontal cortex dopamine and cognition. *eneuro* **8**, https://doi.org/10.1523/eneuro. 0045-21.2021 (2021).
11. Pantoja-Urbán, A. H. et al. Gains and losses: resilience to social defeat stress in adolescent female mice. *Biol. Psychiatry* **95**, 37–47 (2024).
12. Ochi, S. & Dwivedi, Y. Dissecting early life stress-induced adolescent depression through epigenomic approach. *Mol. Psychiatry* **28**, 141–153 (2023).
13. Infurna, M. R. et al. Associations between depression and specific childhood experiences of abuse and neglect: a meta-analysis. *J. Affect. Disord.* **190**, 47–55 (2016).
14. LeMoult, J. et al. Meta-analysis: exposure to early life stress and risk for depression in childhood and adolescence. *J. Am. Acad. Child Adolesc. Psychiatry* **59**, 842–855 (2020).
15. Norman, R. E. et al. The long-term health consequences of child physical abuse, emotional abuse, and neglect: a systematic review and meta-analysis. *PLoS Med.* **9**, e1001349 (2012).
16. Peña, C. J. et al. Early life stress confers lifelong stress susceptibility in mice via ventral tegmental area OTX2. *Science* **356**, 1185–1188 (2017).
17. Cao, P. et al. Early-life inflammation promotes depressive symptoms in adolescence via microglial engulfment of dendritic spines. *Neuron* **109**, 2573–2589.e2579 (2021).
18. Kuhlman, K. R. Pitfalls and potential: Translating the two-hit model of early life stress from pre-clinical non-human experiments to human samples. *Brain Behav. Immun. Health* **35**, 100711 (2024).
19. Uchida, S. et al. Early life stress enhances behavioral vulnerability to stress through the activation of REST4-mediated gene transcription in the medial prefrontal cortex of rodents. *J. Neurosci.* **30**, 15007–15018 (2010).
20. World Health Organization. *WHO Recommendations on Postnatal Care of the Mother and Newborn* (World Health Organization, 2013).
21. Weaver, I. C. et al. Epigenetic programming by maternal behavior. *Nat. Neurosci.* **7**, 847–854 (2004).
22. Weaver, I. C., Meaney, M. J. & Szyf, M. Maternal care effects on the hippocampal transcriptome and anxiety-mediated behaviors in the offspring that are reversible in adulthood. *Proc. Natl. Acad. Sci. USA* **103**, 3480–3485 (2006).
23. Bedrosian, T. A., Quayle, C., Novaresi, N. & Gage, F. H. Early life experience drives structural variation of neural genomes in mice. *Science* **359**, 1395–1399 (2018).
24. Peña, C. J., Nestler, E. J. & Bagot, R. C. Environmental programming of susceptibility and resilience to stress in adulthood in male mice. *Front. Behav. Neurosci.* **13**, 40 (2019).
25. Alizadeh-Ezdini, Z. & Vatanparast, J. Differential impact of two paradigms of early-life adversity on behavioural responses to social defeat in young adult rats and morphology of CA3 pyramidal neurons. *Behav. Brain Res.* **435**, 114048 (2022).
26. Gardner, A. & Boles, R. G. Beyond the serotonin hypothesis: mitochondria, inflammation and neurodegeneration in major depression and affective spectrum disorders. *Prog. Neuro Psychopharmacol. Biol. Psychiatry* **35**, 730–743 (2011).
27. Morava, E. et al. Depressive behaviour in children diagnosed with a mitochondrial disorder. *Mitochondrion* **10**, 528–533 (2010).
28. Zhou, X. Y. et al. Mitochondrial health, NLRP3 inflammasome activation, and white matter integrity in adolescent mood disorders: A pilot study. *J. Affect. Disord.* **340**, 149–159 (2023).
29. Abdallah, C. G. et al. Glutamate metabolism in major depressive disorder. *Am. J. Psychiatry* **171**, 1320–1327 (2014).
30. Dong, W. T. et al. Mitochondrial fission drives neuronal metabolic burden to promote stress susceptibility in male mice. *Nat. Metab.* **5**, 2220–2236 (2023).
31. He, J. G. et al. Transcription factor TWIST1 integrates dendritic remodeling and chronic stress to promote depressive-like behaviors. *Biol. Psychiatry* **89**, 615–626 (2021).
32. Wang, J. et al. A TrkB cleavage fragment in hippocampus promotes Depressive-Like behavior in mice. *Brain Behav. Immun.* **119**, 56–83 (2024).
33. Wang, Y. et al. A tau fragment links depressive-like behaviors and cognitive declines in Alzheimer's disease mouse models through attenuating mitochondrial function. *Front. Aging Neurosci.* **15**, 1293164 (2023).
34. Pantoja-Urbán, A. H., Richer, S., Giroux, M., Nouel, D. & Flores, C. Social defeat stress model for adolescent C57BL/6 male and female mice. *J. Vis. Exp.* https://doi.org/10.3791/66455 (2024).
35. Kessler, R. C. et al. The epidemiology of major depressive disorder: results from the National Comorbidity Survey Replication (NCS-R). *Jama* **289**, 3095–3105, (2003).
36. Pedrelli, P., Shapero, B., Archibald, A. & Dale, C. Alcohol use and depression during adolescence and young adulthood: a summary and interpretation of mixed findings. *Curr. Addict. Rep.* **3**, 91–97 (2016).

37. Song, Y. et al. Mitochondrial dysfunction: a fatal blow in depression. *Biomed. Pharmacother.* **167**, 115652 (2023).

38. Cassidy-Stone, A. et al. Chemical inhibition of the mitochondrial division dynamin reveals its role in Bax/Bak-dependent mitochondrial outer membrane permeabilization. *Dev. Cell* **14**, 193–204 (2008).

39. Zidek, L. M. et al. Deficiency in mTORC1-controlled C/EBPβ-mRNA translation improves metabolic health in mice. *EMBO Rep.* **16**, 1022–1036 (2015).

40. Wang, Z.-H. et al. Neuronal ApoE4 stimulates C/EBPβ activation, promoting Alzheimer's disease pathology in a mouse model. *Prog. Neurobiol.* **209**, 102212 (2022).

41. Ren, Q. et al. C/EBPβ: The structure, regulation, and its roles in inflammation-related diseases. *Biomed. Pharmacother.* **169**, 115938 (2023).

42. Wang, Z. H. et al. ApoE4 activates C/EBPβ/δ-secretase with 27-hydroxycholesterol, driving the pathogenesis of Alzheimer's disease. *Prog. Neurobiol.* **202**, 102032 (2021).

43. Huehnchen, P., Muenzfeld, H., Boehmerle, W. & Endres, M. Blockade of IL-6 signaling prevents paclitaxel-induced neuropathy in C57Bl/6 mice. *Cell Death Dis.* **11**, 45 (2020).

44. Samarasinghe, K. T. G. et al. Targeted degradation of transcription factors by TRAFTACs: TRAnscription Factor TArgeting Chimeras. *Cell Chem. Biol.* **28**, 648–661.e645 (2021).

45. Rombaut, C., Roura-Martinez, D., Lepolard, C. & Gascon, E. Brief and long maternal separation in C57Bl6J mice: behavioral consequences for the dam and the offspring. *Front. Behav. Neurosci.* **17**, 1269866 (2023).

46. Tractenberg, S. G. et al. An overview of maternal separation effects on behavioural outcomes in mice: evidence from a four-stage methodological systematic review. *Neurosci. Biobehav. Rev.* **68**, 489–503 (2016).

47. Rozengurt, E. Mechanistic target of rapamycin (mTOR): a point of convergence in the action of insulin/IGF-1 and G protein-coupled receptor agonists in pancreatic cancer cells. *Front. Physiol.* **5**, 357 (2014).

48. Lee, K. Y. et al. Neonatal repetitive maternal separation causes long-lasting alterations in various neurotrophic factor expression in the cerebral cortex of rats. *Life Sci.* **90**, 578–584 (2012).

49. Middei, S. et al. Early social enrichment modulates tumor progression and p53 expression in adult mice. *Biomolecules* **12**, https://doi.org/10.3390/biom12040532 (2022).

50. Fang, Y. Y., Yamaguchi, T., Song, S. C., Tritsch, N. X. & Lin, D. A hypothalamic midbrain pathway essential for driving maternal behaviors. *Neuron* **98**, 192–207.e110 (2018).

51. Champagne, F. A. Epigenetic mechanisms and the transgenerational effects of maternal care. *Front. Neuroendocrinol.* **29**, 386–397 (2008).

52. Champagne, F., Diorio, J., Sharma, S. & Meaney, M. J. Naturally occurring variations in maternal behavior in the rat are associated with differences in estrogen-inducible central oxytocin receptors. *Proc. Natl. Acad. Sci. USA* **98**, 12736–12741 (2001).

53. Ribeiro, A. C. et al. siRNA silencing of estrogen receptor-α expression specifically in medial preoptic area neurons abolishes maternal care in female mice. *Proc. Natl. Acad. Sci. USA* **109**, 16324–16329 (2012).

54. Dobolyi, A. & Lékó, A. H. The insulin-like growth factor-1 system in the adult mammalian brain and its implications in central maternal adaptation. *Front. Neuroendocrinol.* **52**, 181–194 (2019).

55. Wlodarczyk, A. et al. A novel microglial subset plays a key role in myelinogenesis in developing brain. *EMBO J.* **36**, 3292–3308 (2017).

56. Yao, W. et al. Microglial ERK-NRBP1-CREB-BDNF signaling in sustained antidepressant actions of (R)-ketamine. *Mol. Psychiatry* **27**, 1618–1629 (2022).

57. Lin, R. et al. Directed evolution of adeno-associated virus for efficient gene delivery to microglia. *Nat. Methods* **19**, 976–985 (2022).

58. Wei, H. R. et al. A microglial activation cascade across cortical regions underlies secondary mechanical hypersensitivity to amputation. *Cell Rep.* **43**, 113804 (2024).

59. Bhusal, A. et al. The microglial innate immune protein PGLYRP1 mediates neuroinflammation and consequent behavioral changes. *Cell Rep.* **43**, 113813 (2024).

60. Chen, H. et al. Mitochondrial dynamics dysfunction: Unraveling the hidden link to depression. *Biomed. Pharmacother.* **175**, 116656 (2024).

61. Santos-Silva, T. et al. Transcriptomic analysis reveals mitochondrial pathways associated with distinct adolescent behavioral phenotypes and stress response. *Transl. Psychiatry* **13**, 351 (2023).

62. Calkhoven, C. F., Müller, C. & Leutz, A. Translational control of C/EBPalpha and C/EBPbeta isoform expression. *Genes Dev.* **14**, 1920–1932 (2000).

63. Bégay, V., Baumeier, C., Zimmermann, K., Heuser, A. & Leutz, A. The C/EBPβ LIP isoform rescues loss of C/EBPβ function in the mouse. *Sci. Rep.* **8**, 8417 (2018).

64. Franklin, T. B., Saab, B. J. & Mansuy, I. M. Neural mechanisms of stress resilience and vulnerability. *Neuron* **75**, 747–761 (2012).

65. Gianatiempo, O. et al. Intergenerational transmission of maternal care deficiency and offspring development delay induced by perinatal protein malnutrition. *Nutr. Neurosci.* **23**, 387–397 (2020).

66. Sequeira-Cordero, A., Masís-Calvo, M., Mora-Gallegos, A. & Fornaguera-Trías, J. Maternal behavior as an early modulator of neurobehavioral offspring responses by Sprague-Dawley rats. *Behav. Brain Res.* **237**, 63–70 (2013).

67. Monk, C., Spicer, J. & Champagne, F. A. Linking prenatal maternal adversity to developmental outcomes in infants: the role of epigenetic pathways. *Dev. Psychopathol.* **24**, 1361–1376 (2012).

68. Weaver, I. C. et al. Reversal of maternal programming of stress responses in adult offspring through methyl supplementation: altering epigenetic marking later in life. *J. Neurosci.* **25**, 11045–11054 (2005).

69. Dyer, A. H., Vahdatpour, C., Sanfeliu, A. & Tropea, D. The role of Insulin-Like Growth Factor 1 (IGF-1) in brain development, maturation and neuroplasticity. *Neuroscience* **325**, 89–99 (2016).

70. Lee, Y. M. et al. Microbiota control of maternal behavior regulates early postnatal growth of offspring. *Sci. Adv.* **7**, https://doi.org/10.1126/sciadv.abe6563 (2021).

71. Ouni, M., Belot, M. P., Castell, A. L., Fradin, D. & Bougnères, P. The P2 promoter of the IGF1 gene is a major epigenetic locus for GH responsiveness. *Pharmacogenomics J.* **16**, 102–106 (2016).

72. Kantake, M. et al. IGF1 gene is epigenetically activated in preterm infants with intrauterine growth restriction. *Clin. Epigenetics* **12**, 108 (2020).

73. Umayahara, Y. et al. CCAAT/enhancer-binding protein delta is a critical regulator of insulin-like growth factor-I gene transcription in osteoblasts. *J. Biol. Chem.* **274**, 10609–10617 (1999).

74. Aghanoori, M. R. et al. CEBPβ regulation of endogenous IGF-1 in adult sensory neurons can be mobilized to overcome diabetes-induced deficits in bioenergetics and axonal outgrowth. *Cell. Mol. Life Sci.* **79**, 193 (2022).

75. Feldman, R., Braun, K. & Champagne, F. A. The neural mechanisms and consequences of paternal caregiving. *Nat. Rev. Neurosci.* **20**, 205–224 (2019).

76. Strekalova, T., Spanagel, R., Bartsch, D., Henn, F. A. & Gass, P. Stress-induced anhedonia in mice is associated with deficits in forced swimming and exploration. *Neuropsychopharmacology* **29**, 2007–2017 (2004).

77. Alves-Dos-Santos, L., Resende, L. S. & Chiavegatto, S. Susceptibility and resilience to chronic social defeat stress in adolescent male

mice: No correlation between social avoidance and sucrose pre-ference. *Neurobiol. Stress* **12**, 100221 (2020).

78. Ochsner, S. A. et al. The Signaling Pathways Project, an integrated 'omics knowledgebase for mammalian cellular signaling pathways. *Sci. Data* **6**, 252 (2019).

79. Mei, S. et al. Cistrome Data Browser: a data portal for ChIP-Seq and chromatin accessibility data in human and mouse. *Nucleic Acids Res.* **45**, D658–d662 (2017).

80. Rauluseviciute, I. et al. JASPAR 2024: 20th anniversary of the open-access database of transcription factor binding profiles. *Nucleic Acids Res.* **52**, D174–d182 (2024).

81. Andersen, S. L. Exposure to early adversity: points of cross-species translation that can lead to improved understanding of depression. *Dev. Psychopathol.* **27**, 477–491 (2015).

82. Andersen, S. L., Lyss, P. J., Dumont, N. L. & Teicher, M. H. Enduring neurochemical effects of early maternal separation on limbic structures. *Ann. N. Y. Acad. Sci.* **877**, 756–759 (1999).

83. Weiss, I. C., Domeney, A. M., Heidbreder, C. A., Moreau, J. L. & Feldon, J. Early social isolation, but not maternal separation, affects behavioral sensitization to amphetamine in male and female adult rats. *Pharmacol. Biochem. Behav.* **70**, 397–409 (2001).

84. Oddi, D. et al. Early social enrichment rescues adult behavioral and brain abnormalities in a mouse model of Fragile X syndrome. *Neuropsychopharmacology* **40**, 1113–1122 (2015).

85. Xu, C., Peng, B. & Liu, S. Using intra-brain drug infusion to investigate neural mechanisms underlying reward-seeking behavior in mice. *STAR Protoc.* **3**, 101221 (2022).

86. Bordt, E. A. et al. Isolation of microglia from mouse or human tissue. *STAR Protoc.* **1**, https://doi.org/10.1016/j.xpro.2020.100035 (2020).

87. Huang, S. et al. Disruption of the Na(+)/K(+)-ATPase-purinergic P2X7 receptor complex in microglia promotes stress-induced anxiety. *Immunity* **57**, 495–512.e411 (2024).

88. Chen, H. et al. Microglial glutaminase 1 mediates chronic restraint stress-induced depression-like behaviors and synaptic damages. *Signal Transduct. Target. Ther.* **8**, 452 (2023).

Acknowledgements

Author contributions

H.Y.C., R.F.X., J.H.W., and F.G. contributed equally to this work. Z.-H.W. conceptualized and designed all studies. H.Y.C., J.H.W., F.G., Y.D.L., X.L., F.L. J.Q.Z., and X.-Y.G performed and analyzed the behavioral tests and molecular experiments. X.Z., J.B.W., R.C.D., Y.K.S., H.Y., S.D., W.X.L., R.F.X., and F.G. conducted animal treatment, virus injection, and drug delivery. J.X., J.Z., and L.Z. conducted bioinformatic analysis and transcription factor prediction. The paper was written by H.Y.C., R.F.X., J.H.W., F.G., and Z.-H.W.

Competing interests

The authors declare no competing interests.

Additional information

Supplementary information The online version contains supplementary material available at https://doi.org/10.1038/s41467-025-57810-w.

Correspondence and requests for materials should be addressed to Zhi-Hao Wang.

Peer review information *Nature Communications* thanks Ioana Carcea and the other anonymous reviewer(s) for their contribution to the peer review of this work. A peer review file is available.

Reprints and permissions information is available at http://www.nature.com/reprints

Publisher's note Springer Nature remains neutral with regard to jurisdictional claims in published maps and institutional affiliations.